Genetic Evidence for the Involvement of Mismatch Repair Proteins, PMS2 and MLH3, in a Late Step of Homologous Recombination.

Md Maminur Rahman, Mohiuddin Mohiuddin, Islam Shamima Keka, Kousei Yamada, Masataka Tsuda, Hiroyuki Sasanuma, Jessica Andreani, Raphael Guerois, Valérie Borde, Jean-Baptiste Charbonnier, et al.

Genetic Evidence for the Involvement of Mismatch Repair Proteins, PMS2 and MLH3, in a Late Step of Homologous Recombination

Md Maminur Rahman[1,†], Mohiuddin Mohiuddin[1,#,†], Islam Shamima Keka[1,#], Kousei Yamada[1], Masataka Tsuda[1,§], Hiroyuki Sasanuma[1], Jessica Andreani[2], Raphael Guerois[2], Valerie Borde[3], Jean-Baptiste Charbonnier[2], and Shunichi Takeda[1]*

[1]Department of Radiation Genetics, Graduate School of Medicine, Kyoto University, Yoshida-Konoe-cho, Kyoto 606-8501, Japan.

[2]Université Paris-Saclay, CEA, CNRS, Institute for Integrative Biology of the Cell (I2BC), 91198, Gif-sur-Yvette, France

[3]Institut Curie, PSL Research University, CNRS UMR3244, Paris, France.

[#]Present address: Program of Genetics and Genome Biology, The Hospital for Sick Children, Toronto, Ontario M5G 1L7, Canada

[§]Present address: Program of Mathematical and Life Science, Graduate School of Integrated Sciences for Life, Hiroshima University, 1-3-1 Kagamiyama, Higashi-Hiroshima 739-8526, Japan

[†]M.M. Rahman and M. Mohiuddin contributed equally to the work.

*To whom correspondence should be addressed. Tel: +81-75-753-4410; Fax: +81-75-753-4419; Email: stakeda@rg.med.kyoto-u.ac.jp

Running title: **Role of PMS2 and MLH3 in Homologous Recombination**

Keywords: Homologous Recombination; PMS2, MLH3, MLH1, MUS81, GEN1, Resolvase, Joint Molecules.

Abstract

Homologous recombination (HR) repairs DNA double-strand breaks (DSBs) using intact homologous sequences as template DNA. Broken DNA and intact homologous sequences form joint molecules (JMs), including Holliday junctions (HJs), as HR intermediates. HJs are resolved to form crossover and noncrossover products. A mismatch repair factor, MLH3 endonuclease produces the majority of crossovers during meiotic HR. It remains elusive whether mismatch repair factors promote HR in non meiotic cells. We disrupted genes encoding the MLH3 and PMS2 endonucleases in the human B cell line, TK6, generating null *MLH3*$^{-/-}$ and *PMS2*$^{-/-}$ mutant cells. We also inserted point mutations into the endonuclease motif of *MLH3* and *PMS2* genes, generating *MLH3*$^{DN/DN}$ and *PMS2*$^{EK/EK}$ cells. *MLH3*$^{-/-}$ and *MLH3*$^{DN/DN}$ cells showed a very similar phenotype, 2.5 times decrease in the frequency of heteroallelic HR-dependent repair of a restriction-enzyme-induced DSBs. *PMS2*$^{-/-}$ and *PMS2*$^{EK/EK}$ cells showed a phenotype very similar to that of the MLH3 mutants. These data indicate that MLH3 and PMS2 promote HR as an endonuclease. The *MLH3*$^{DN/DN}$ and *PMS2*$^{EK/EK}$ mutations had an additive effect on the heteroallelic HR. *MLH3*$^{DN/DN}$/*PMS2*$^{EK/EK}$ cells showed normal kinetics of γ-irradiation-induced Rad51 foci but a significant delay in the resolution of Rad51 foci and three times decrease in the number of cisplatin-induced sister chromatid exchange (SCE). The ectopic expression of the Gen1 HJ resolvase partially reversed the defective heteroallelic HR of *MLH3*$^{DN/DN}$/*PMS2*$^{EK/EK}$ cells. We propose that MLH3 and PMS2 promote HR as endonucleases, most likely by processing JMs in mammalian somatic cells.

Introduction

The mismatch repair (MMR) pathway corrects the mismatch formed during DNA replication (1–5). MMR is initiated by the recognition of mismatches by the heterodimers, MSH2-MSH6 (MutSα), and MSH2-MSH3 (MutSβ) (5–10). Upon recognition, the MutS heterodimers interact with one of the three MutL heterodimers, MLH1-PMS2 (MutLα), MLH1-PMS1 (MutLβ), and MLH1-MLH3 (MutLγ) (11–13). A single-strand break formed by the MLH1-PMS2 endonuclease serves as entry points for the exonuclease activity that removes mismatched DNA. The endonuclease activity of MLH1-PMS2 depends on the metal-binding motif $DQHA(X)_2E(X)_4E$ present on PMS2 and the last ten residues of MLH1 (14). This nuclease-active site is conserved in MLH3 but not in PMS1 (15).

A subclass of the MMR proteins is involved in double-strand break (DSB) repair. Firstly, MutS complexes play a role in the rejection of heteroduplex DNA containing insertion/deletion mismatches when the nucleotide sequences of two partner DNAs are not identical (16, 17). Second, MutSα may recognize mismatches within the heteroduplex region of the JMs and avoid recombination, collaborating with RecQ helicases (18). Third, MLH1 can affect nonhomologous end-joining (NHEJ) (19), which repairs 80% of the ionizing-radiation-induced DSB in the G2 phase (20). Forth, a subset of MSH and MLH proteins promote meiotic HR, which function is distinct from their MMR functions. MLH1-MLH3, which has a minor role in MMR, is critical for producing meiotic crossover products in mice and *Saccharomyces cerevisiae* (*S. cerevisiae*) (21, 22). MLH1, MLH3, and PMS2 are essential for the progression of meiotic HR in mice (23–28). The role played by the putative endonuclease activity of PMS2 in the resolution of meiotic HR intermediates has not yet been clarified in the mouse or human but recent studies have unveiled new insights into the molecular mechanisms of MLH1-MLH3 and the role of its endonuclease activity (29, 30). Another unsolved question is whether MLH3 and PMS2 promote HR in mammalian somatic cells.

HR initiates DSB repair by resecting DSBs leading to the formation of 3′ single-strand overhangs, followed by polymerization of Rad51 on the single-strand DNA (31–33). The resulting Rad51 nucleoprotein filaments undergo homology search and pairing with the intact duplex DNA donor to form joint molecules (JMs) such as double Holliday junctions (dHJs) with the help of Rad54 (33–35). JMs are resolved into individual DNA duplexes to allow chromosomes to separate in the anaphase. The separation is performed by two alternative processes, the dissolution and resolution

pathways. The phenotypic analysis of meiotic HR indicates that only 10% of the DSBs (*M. musculus*) form dHJs, and these are almost exclusively processed by the resolution pathway, involving the activity of MLH1-MLH3 (22). In somatic cells, the resolution of HJs is done by a number of structure-specific endonucleases, MUS81-EME1, SLX1-SLX4, XPF-ERCC1, and GEN1 (36–39). Mice deficient in either MUS81-EME1 or SLX1-SLX4 or GEN1 are all viable, whereas mice deficient in both MUS81-EME1 and GEN1 are synthetic lethal (40–43), suggesting a substantial functional overlap between the two nucleases. Although yeast genetic studies have precisely monitored the formation of HR intermediate molecules such as HJs over time upon DSB formation during both meiosis and mitosis (21, 34, 44, 45), no equivalent phenotypic assays are available in the phenotypic analysis of HR in mammalian somatic cells.

There are two major DSB repair pathways in mammalian cells, HR and nonhomologous end-joining (NHEJ). The two pathways differentially contribute to cellular tolerance to anti-malignant therapies. These pathways contribute to tolerance to radiotherapy with HR functioning in the S to G2 phases and NHEJ functioning in the whole cell cycle (46). HR, but not NHEJ, repairs DSBs induced by camptothecin (Top1 poison) and olaparib (poly[ADP ribose]polymerase poison). NHEJ plays the dominant role in repairing DSBs induced by ICRF-193 (catalytic inhibitor of Top2) (47, 48). Thus, the sensitivity profile of DSB-repair mutants to these chemotherapeutic agents help to discriminate which repair pathway is compromised in the mutants.

To investigate the role for MLH3 and PMS2 as nucleases in DSB repair of somatic mammalian cells, we inserted point mutation into the DQHA$(X)_2$E$(X)_4$E motif of the endogenous *MLH3* and *PMS2* genes of the human TK6 B cell line (49) and generated $MLH3^{D1223N/D1223N}$ and $PMS2^{E705K/E705K}$ cells. These mutants exhibited increased sensitivities to camptothecin and olaparib, a few times decrease in the frequency of both SCE and the heteroallelic HR, and delayed resolution of γ-ray-induced Rad51 foci, indicating a defect in HR in later steps. Surprisingly, their role seems to be mostly independent of MLH1. We conclude that the MLH3 and PMS2 proteins promote DSB repair by HR presumably by processing JMs in human cells.

Results

MLH3 and PMS2 mutants, but not MSH2 and MLH1 mutants, are sensitive to both camptothecin and olaparib

We disrupted the *PMS2* and *MLH3* genes in TSCER2 cells (50, 51), a TK6 sub-line for measuring heteroallelic HR, generating *PMS2*$^{-/-}$ and *MLH3*$^{-/-}$ cells (Figures S1 and S2). We also generated *MSH2*$^{-/-}$ cells (Figures S3A and B), as MSH2 plays a major role in MMR but is not involved in the resolution of HJs in *S. cerevisiae* (21). *MSH2*$^{-/-}$ cells were tolerant to an alkylating agent, temozolomide (Figure S3C), as expected from a defect in MMR (52). *PMS2*$^{-/-}$ and *MLH3*$^{-/-}$ cells were sensitive to camptothecin, γ-irradiation, and olaparib (Figures 1A and B), whereas *MSH2*$^{-/-}$ cells were tolerant to these damaging agents (Figures S3D, E, and F). These data suggest the involvement of PMS2 and MLH3 in HR-dependent DSB repair independently of their functioning in MMR or independently of their interaction with MutSα (MSH2-MSH6) or MutSβ (MSH2-MSH3) heterodimers. We generated *MLH1*$^{-/-}$ cells (Figure S4) and verified a defect in MMR by confirming the marked tolerance to temozolomide (53) (Figure S4F). We found no noticeable sensitivity of *MLH1*$^{-/-}$ cells to γ-irradiation (Figure 1A). We disrupted the *MUS81* gene in *wild-type* and *PMS2*$^{-/-}$ TK6 clones (Figure S5). The resulting *MUS81*$^{-/-}$ cells showed a phenotype very similar to that of *PMS2*$^{-/-}$ cells. *MUS81*$^{-/-}$*/PMS2*$^{-/-}$ cells showed higher sensitivity to olaparib than *MUS81*$^{-/-}$ and *PMS2*$^{-/-}$ cells (Figure 1C). These observations support the notion that PMS2 and MUS81 act independently of each other in HR-mediated DSB repair.

To investigate the catalytic role of MLH3 and PMS2, we inserted point mutations into the endogenous *MLH3* and *PMS2* genes at the highly conserved $DQHA(X)_2E(X)_4E$ metal-binding motif. The replacement of the glutamic acid residue in position 705 by lysine (E705K) in human PMS2 completely inactivates its endonuclease activity (15, 54, 55). Likewise, the D523N and E529K mutations in *S. cerevisiae* MLH3, which correspond to the D1223N and E1229K mutations in human MLH3, impair both MMR and the resolution of JMs in meiotic HR in mice and *Saccharomyces cerevisiae* (21, 22, 56–59). We thus generated *PMS2*$^{E705K/E705K}$ cells (Figure S1), and *MLH3*$^{D1223N/D1223N}$ and *MLH3*$^{E1229K/E1229K}$ cells (Figure S6). These mutants are hereafter written as *PMS2*$^{EK/EK}$, *MLH3*$^{DN/DN}$, and *MLH3*$^{EK/EK}$ cells. The sensitivity profile of *PMS2* $^{EK/EK}$ cells was the same as that of *PMS2*$^{-/-}$ cells (Figure 1A). Likewise, *MLH3*$^{-/-}$, *MLH3*$^{DN/DN}$, and *MLH3*$^{EK/EK}$ cells showed the same phenotype (Figure 1B). These observations suggest that PMS2 and MLH3 contribute to HR mediated DSB repair as the endonuclease.

The repair of γ-ray-induced DSBs during G2 phase is severely compromised in the PMS2 and MLH3 mutant cells

To monitor DSB repair selectively during the G2 phase when HR is active, we exposed cells to ionizing-radiation and measured the number of chromosomal aberrations in mitotic chromosome spreads at three hours after ionizing-radiation. Only cells that were γ-irradiated at the G2 phase, but not S phase, can enter the M phase within three hours (60). This method allows for evaluating the capability of HR to repair DSBs with several times higher sensitivity than the analysis of the γ-irradiation-sensitivity of asynchronous cell populations (Figures 1A and B). Indeed, γ-irradiation increased the number of chromosomal breaks by 1.0 per *MUS81*$^{-/-}$ cell and only 0.2 per *wild-type* cell (Figure 2B). Remarkably, the total numbers of chromosome aberrations induced by γ-rays were around ten times higher in the PMS2 and MLH3 mutant cells in comparison with *wild-type* cells (Figure 2B). The total number of mitotic chromosome aberrations was significantly higher in *MLH1*$^{-/-}$ cells, but not in *MSH2*$^{-/-}$ cells, in comparison with *wild-type* cells (Figure 2B). We conclude no significant contribution of canonical MMR involving MSH2 to DSB repair during the G2 phase. The total numbers of γ-ray-induced chromosome aberrations increased to very similar extents in the five mutants, *PMS2*$^{-/-}$, *PMS2*$^{EK/EK}$, *MLH3*$^{-/-}$, *MLH3*$^{DN/DN}$, and *MLH3*$^{EK/EK}$ cells (Figure 2B). These data suggest that PMS2 and MLH3 significantly contribute to DSB repair as endonuclease.

We counted the number of chromosome aberrations distinguishing chromatid-type breaks (one of the two sister chromatids is broken), isochromatid-type breaks (two sister chromatids are broken at the same sites) and radial chromosomes (comprise the association of two or more chromatids) (Figure 2A). Ionizing irradiation of *RAD54*$^{-/-}$ cells caused a more significant increase in the number of chromatid-type breaks than that of isochromatid-type breaks (Figure 2B). This observation agrees with the role of RAD54 in promoting strand exchange and JM formation. In contrast, *MUS81*$^{-/-}$ cells showed marked increases in the numbers of isochromatid-type breaks. Isochromatid-type breaks result from abnormal processing of JMs between broken and intact sister chromatids, as the persistent presence of JMs interferes with local chromosome condensation of both sister chromatids, leading to microscopically visible breakage of the two chromosomes at the same sites (39, 61, 62). Radial chromosomes may be caused by the abnormal separation of JMs containing two sisters, leading to inverted chromosome fusions. Like *MUS81*$^{-/-}$ cells, the PMS2 and MLH3 mutants showed significant increases in the numbers of both isochromatid-type breaks and radial chromosomes (Figure 2B). These data suggest that PMS2 and MLH3 promote HR-dependent DSB repair after formation of JMs as does MUS81.

Surprisingly, the *MLH1*$^{-/-}$ phenotype is not as severe as expected from the phenotypes of the PMS2 and MLH3 mutants, particularly no significant alteration regarding isochromatid-type breaks. A moderate increase in the number of chromatid-type breaks in *MLH1*$^{-/-}$ cells suggests that the MLH1-MLH3 and MLH1-PMS2 heterodimers may play a minor role in NHEJ-mediated DSB repair, as suggested previously (19). One possible scenario is that an MLH1-independent alternative mechanism of PMS2 and MLH3 might be present in the process observed in this study. These data suggest that PMS2 and MLH3 promote HR-dependent DSB repair after the formation of JMs, as does MUS81.

PMS2$^{EK/EK}$*/MLH3*$^{DN/DN}$ *double mutant cells display stronger HR defects than PMS2*$^{EK/EK}$ *and MLH3*$^{DN/DN}$ *cells*

We chose *MLH3*$^{DN/DN}$ cells as a representative MLH3 mutant due to the phenotypic similarity among *MLH3*$^{-/-}$, *MLH3*$^{DN/DN}$, and *MLH3*$^{EK/EK}$ cells. Likewise, we chose *PMS2*$^{EK/EK}$ cells for the subsequent analyses. To investigate the functional relationship between the PMS2 and MLH3 endonucleases, we generated *PMS2*$^{EK/EK}$*/MLH3*$^{DN/DN}$ double mutant cells. The doubling time was 12.5 hours for *wild-type*, 12.7 hours for *PMS2*$^{EK/EK}$, 12.7 hours for *MLH3*$^{DN/DN}$, and 14.3 hours for *PMS2*$^{EK/EK}$*/MLH3*$^{DN/DN}$ cells. The plating efficiency of these cells was 50 to 60% for all genotypes. *PMS2*$^{EK/EK}$*/MLH3*$^{DN/DN}$ cells showed high sensitivity to camptothecin and γ-rays, higher than *MLH3*$^{DN/DN}$, and slightly higher than *PMS2*$^{EK/EK}$, suggesting a prominent role of PMS2 in these assays Figure 1D). *PMS2*$^{EK/EK}$*/MLH3*$^{DN/DN}$ cells also showed a higher sensitivity to olaparib than did *PMS2*$^{EK/EK}$ and *MLH3*$^{DN/DN}$ cells (Figure 1D). The number of γ-ray-induced chromosomal breaks was more than 50% higher in *PMS2*$^{EK/EK}$*/MLH3*$^{DN/DN}$ cells than in *PMS2*$^{EK/EK}$ and in *MLH3*$^{DN/DN}$ cells (Figure 2). We, therefore, conclude that PMS2 and MLH3 contribute to HR as the endonuclease independently of each other.

We monitored DSB repair kinetics by measuring the number of γH2AX foci with time after γ-irradiation (Figure 3). The numbers of γH2AX foci were very similar among *MLH3*$^{DN/DN}$, *PMS2*$^{EK/EK}$, and *wild-type* cells at two hours after ionizing irradiation. The numbers of γH2AX foci reduced more slowly in *MLH3*$^{DN/DN}$ and *PMS2*$^{EK/EK}$ cells in comparison with *wild-type* and *MLH1*$^{-/-}$ cells (Figure 3). The delayed DSB repair kinetics observed more than two hours after ionizing irradiation is consistent with the fact that HR needs a longer time to complete DSB repair than does NHEJ (20). *PMS2*$^{EK/EK}$*/MLH3*$^{DN/DN}$ cells showed a more prominent delay in DSB repair at 8 hours

in comparison with *MLH3*$^{DN/DN}$ and *PMS2*$^{EK/EK}$ cells (Figure 3). We conclude that PMS2 and MLH3 promote DSB repair independently of each other in an MLH1-independent manner.

Resolution of γ-ray-induced RAD51 foci is delayed in the PMS2 and MLH3 mutant cells

To evaluate if PMS2 and MLH3 act in the early and late steps of HR, we analyzed the formation of Rad51 foci over time after γ-irradiation (Figure 4). The number of Rad51 foci peaked at two hours after γ-irradiation in *wild-type* TK6 cells (60). *MLH3*$^{DN/DN}$, *PMS2*$^{EK/EK}$, and *PMS2*$^{EK/EK}$*/MLH3*$^{DN/DN}$ cells showed the same extent of Rad51 foci at two hours as *wild-type* cells. Thus, PMS2 and MLH3 are dispensable for DSB resection and the polymerization of Rad51 on resected DSBs. Remarkably, *MLH3*$^{DN/DN}$, *PMS2*$^{EK/EK}$, and *PMS2*$^{EK/EK}$*/MLH3*$^{DN/DN}$ cells showed a significant delay in the resolution of Rad51 foci in comparison with *wild-type* and *MLH1*$^{-/-}$ cells (Figure 4). Both *MLH3*$^{DN/DN}$ and *PMS2*$^{EK/EK}$ single mutants showed a similar delay in the resolution of Rad51 foci in comparison with *MUS81*$^{-/-}$ cells, but this effect was more prominent in the *PMS2*$^{EK/EK}$*/MLH3*$^{DN/DN}$ double mutant cells (Figure 4B). All mutants were less sensitive than *RAD54*$^{-/-}$ cells. We, therefore, conclude that the PMS2 and MLH3 endonucleases promote HR-dependent DSB repair after the polymerization of Rad51 at DSBs.

MLH3*$^{DN/DN}$ *and PMS2*$^{EK/EK}$ *cells are deficient in heteroallelic HR

To assess the involvement of PMS2 and MLH3 in the resolution of HJs, we measured the frequency of heteroallelic recombination between the allelic thymidine kinase (*TK*) genes carrying compound heterozygous mutations (47, 50, 60, 63) (Figure 5A). One of the two allelic *TK* genes carries an I-*Sce*1 site, and a mutation in the exon 5 localizes 108 nucleotides downstream of the I-*Sce*1 site. When I-*Sce*1-induced DSBs are repaired by either the gene conversion (HR) that associates with crossover or long-tract gene conversion, it can restore an intact *TK* gene. These restoration events are detectable by counting the frequency of drug-resistant colonies (50). The HR frequency was 60% smaller in *MUS81*$^{-/-}$ cells compared with *wild-type* cells (Figure 5B), suggesting that a majority of the heteroallelic recombination events involve the formation of HJs. The PMS2 and MLH3 mutants, including *MLH3*$^{DN/DN}$ and *PMS2*$^{EK/EK}$ cells, showed 60-70% decreases, and *PMS2*$^{EK/EK}$*/ MLH3*$^{DN/DN}$ and *MUS81*$^{-/-}$*/PMS2*$^{-/-}$ cells showed further declines in the frequency of crossover events when compared with *wild-type* cells (Figure 5B). These observations suggest that the endonuclease-activity of PMS2 and MLH3 may be involved in the resolution of HJs. This function of PMS2 and MLH3 is also independent of MLH1 and MSH2.

We further assessed the involvement of PMS2 and MLH3 in the resolution of HJs by measuring SCE events, crossover-type HR (62, 64, 65). To induce SCE, we treated cells with cisplatin, an interstrand crosslinking agent. The number of cisplatin-induced SCE events was measured by subtracting the number of SCE before cisplatin-treatment from the number of SCE post-treatment (Figure 5C and 5D). The treatment increased the SCE frequency by 11 events per 100 mitotic *wild-type* cells (Figure 5D). The number of induced SCE was 50% smaller in *MUS81*$^{-/-}$ cells when compared with *wild-type* cells. *MLH3*$^{DN/DN}$ and *PMS2*$^{EK/EK}$ cells also showed 50% decreases, and *PMS2*$^{EK/EK}$*/MLH3*$^{DN/DN}$ cells showed an 80% decrease in the SCE in comparison with *wild-type* cells (Figure 5C and 5D). In summary, PMS2 and MLH3 contribute to crossover formation most likely by promoting the resolution of HJs, as does MUS81, but MLH1 is not involved in this process.

The loss of MLH1 does not impair HR-dependent DSB repair

MLH1 physically interacts with PMS2 and MLH3 as heterodimers and thereby stabilizes the two endonucleases (66). Here to evaluate the role of MLH1 in the mitotic HR we have employed five phenotypic assays, (i) sensitivity to camptothecin, γ-irradiation and olaparib (Figure 1A), (ii) γ-ray-induced chromosome aberrations (Figure 2B), (iii) measuring the number of γH2AX and Rad51 foci over time after γ-irradiation (Figure 3 and 4), (iv) measuring the frequency of the heteroallelic recombination (Figure 5A and 5B), and (v) SCE induced by cisplatin (Figure 5C and 5D). Unexpectedly, as mentioned above, all of these phenotypic assays consistently showed that *MLH1*$^{-/-}$ cells were proficient in HR-mediated DSB repair. We, therefore, conclude that MLH1 is dispensable for the functioning of human MLH3 and PMS2 in mitotic HR. It represents to our knowledge the first example, where MLH1 is not required for the functioning of MLH3 and PMS2. Indeed, MLH1 has been shown to be required for the functioning of MLH3 and PMS2 in MMR and in meiotic HR in mice (24, 25).

We speculated that the MLH1-independent function of PMS2 and MLH3 in mitotic HR can be achieved through I) homodimer formation, II) forming heterodimer with unknown partner protein which stabilize the PMS2 and MLH3 proteins, and III) MLH3-PMS2 heterodimer. We could not examine these possibilities due to the lack of specific antibodies and no appropriate method of inserting functional tag sequences into PMS2 and MLH3. We therefore investigated PMS2 and MLH3 homodimer and heterodimer formation through 3D-structure modeling using a standard

homology modeling pipeline based on the HHpred and RosettaCM methods (67–69). Structural analysis of the resulting models supports the potential homodimer and heterodimer formation (Figure S8A, S8B, and S8C).

Significant rescue of the defective HR of the MLH3 and PMS2 mutants by ectopic expression of GEN1.

We reason that if the PMS2 and MLH3 endonuclease activities promote HR by processing HJs, the mutant phenotype of *MLH3*$^{DN/DN}$ and *PMS2*$^{EK/EK}$ cells could be suppressed by ectopic expression of one of the resolvases described for HJs. We chose GEN1 as the HJ resolvase (70), and used the *GEN1* transgene carrying mutations in its nuclear export signal (NES) and fused with the nuclear localization signal (NLS) (71) (Figure 6A). We added the FLAG tag to this *GEN1* transgene and inserted it into the pMSCV retroviral expression vector, which allows for the bi-cistronic expression of the *GFP* and *GEN1* transgenes (72) (Figure S7). We produced recombinant retrovirus and infected them into TK6 clones. To confirm the expression of the transgene, we performed western blot analyses using an anti-flag antibody (Figure S7D). We measured the ionizing-radiation sensitivity and calculated LD50, the dose of γ-rays that reduced the survival of cells to 50% relative to non-irradiated cells (Figure 6B). The expression of the *GEN1* transgene reversed the ionizing-radiation sensitivity of *MUS81*$^{-/-}$ cells, but not *wild-type* or *RAD54*$^{-/-}$ cells. Thus, the *GEN1* transgene is able to selectively normalize the defective processing of JMs during HR mediated DSB repair.

The *GEN1* transgene restored the tolerance of *MLH3*$^{DN/DN}$, *PMS2*$^{EK/EK}$, and *PMS2*$^{EK/EK}$/*MLH3*$^{DN/DN}$ cells to γ-rays at least partially (Figure 6B). The rescue effect of *GEN1* transgene was more efficient in *PMS2*$^{EK/EK}$/*MLH3*$^{DN/DN}$ double mutant cells compare to *MLH3*$^{DN/DN}$ and *PMS2*$^{EK/EK}$ cells. In agreement with this finding, the *GEN1* transgene significantly reduced the total number of chromosomal aberrations in these mutants as well as *MUS81*$^{-/-}$ cells (Figure 6C). Importantly, the *GEN1* transgene expression reduced the number of isochromatid-type breaks to a considerably greater extent than that of chromatid breaks (Figure 6C). The *GEN1* transgene increased the frequency of heteroallelic HR in *MUS81*$^{-/-}$ cells by 60% but had no effect on that in *wild-type* or *RAD54*$^{-/-}$ cells (Figure 6D), suggesting that a substantial fraction of heteroallelic HR involves HJ formation as HR intermediates. The *GEN1* transgene restored heteroallelic HR in *MLH3*$^{DN/DN}$, *PMS2*$^{EK/EK}$, *PMS2*$^{EK/EK}$/*MLH3*$^{DN/DN}$, as well as *MUS81*$^{-/-}$ cells but not *wild-type* or *RAD54*$^{-/-}$ cells

(Figure 6D). In summary, the PMS2 and MLH3 endonuclease activities facilitate the separation of HJs.

Discussion

We demonstrate that human PMS2 and MLH3 promote DSB repair by HR in human somatic cells. Previous studies failed to uncover their role in the repair of X-ray-induced DSBs, presumably because murine primary cells deficient in PMS2 are slightly resistant to ionizing radiation due to defective MMR of damaged nucleotides (73). Strikingly, the defective HR phenotype of the PMS2 and MLH3 mutants derived from the TK6 cell line was as prominent as that of TK6 cells deficient in MUS81, an important endonuclease involved in the resolution of HJs (36, 37) (Figures 2B, 5B, 5C, and 5D). Furthermore, $PMS2^{EK/EK}/MLH3^{DN/DN}$ cells displayed a significantly stronger phenotype than did $MUS81^{-/-}$ cells, including 15 times more mitotic chromosome breaks induced by γ-irradiation at the G2 phase (Figure 2B) and ~80% decrease in the number of cisplatin-induced sister chromatic exchanges (Figure 5C and 5D) in comparison with *wild-type* cells. The contribution of PMS2 and MLH3 to HR is totally independent of their functioning in MMR since MSH2 and MLH1 are required for MMR but dispensable for HR (Figure 2). In summary, human PMS2 and MLH3 significantly contribute to the genome stability of somatic cells through at least two distinct mechanisms; MMR and DSB repair by HR.

The present study shows compelling genetic evidence for the requirement of the PMS2 and MLH3 endonuclease activity for the efficient resolution of HJs. $MLH3^{DN/DN}$ and $MLH3^{-/-}$ cells showed the same phenotype in the defective HR **(**Figure 2). Likewise, the phenotype of $PMS2^{EK/EK}$ cells was very similar to that of $PMS2^{-/-}$ cells **(**Figure 2). These data indicate PMS2 and MLH3 promote HR as the endonuclease. In the $MLH3^{DN/DN}$ and $PMS2^{EK/EK}$ mutants, the initial kinetics of γ-ray-induced RAD51 focus formation was normal, whereas its resolution was significantly delayed (Figure 4). We, therefore, conclude that the PMS2 and MLH3 endonuclease activities promote a late step of HR, most likely after the formation of JMs. The $MUS81^{-/-}$, $MLH3^{DN/DN}$, and $PMS2^{EK/EK}$ mutants all showed a ~40% decrease in the frequency of cisplatin-induced SCEs (Figure 5D). Furthermore, ectopic expression of GEN1, a typical HJ resolvase, reversed the defective heteroallelic HR of $MUS81^{-/-}$, $MLH3^{DN/DN}$, and $PMS2^{EK/EK}$ cells by 30% - 50% (Figure 6). In conclusion, the endonuclease activity of PMS2 and MLH3 process HJs generating both crossover and noncrossover products.

The PMS2-MLH1 and MLH3-MLH1 heterodimers are involved in both MMR and meiotic HR in *S. cerevisiae* and mice (21, 24, 25, 66). Unexpectedly, we observed that only PMS2 and MLH3, but not MLH1, are involved in HR in human somatic cells. The PMS2 and MLH3 proteins may form homodimers and heterodimers when they are involved in HR in the same manner as the MutL homologs form heterodimer mediated by their C-terminal region (14). Indeed, homodimers of yeast Mlh1 have been reported, and an increase of their formation can inhibit MMR (74). In addition, in support of a possible heterodimer formation, a recent study in budding yeast found co-immunoprecipitation of Mlh3 with Pms1 (the equivalent of PMS2) (ref59 BioRxiv). The crystal structure of the C-terminal region of human MLH1 (pdb code 3RBN) showed that human MLH1 could form homodimers with the same residues involved in the heterodimer formation (14). The HHpred and RosettaCM analysis also suggested that the homodimer as well as heterodimer formation is possible (Figure S8). Future studies will demonstrate the homodimer and heterodimer formation as well as the interaction with an unidentified partner protein.

MLH3 and PMS2 have strong tumor suppressor activities, and it is believed that these activities are attributable exclusively to their functioning of MMR (75). The current study suggests that these endonucleases may contribute to tumor suppression also by promoting the resolution of HJs. The MUS81-EME1, SLX1-SLX4, and GEN1 endonucleases all play the critical role in genome maintenance particular when Bloom helicase is attenuated (62, 76, 77). Nonetheless, it remains unclear how much these endonucleases contribute to tumor suppression in the human. A defect in the resolution of HJs can pose a more serious threat to genome stability in comparison with the initial step of HR because the former deficiency not only leaves DSBs unrepaired but also can cleave intact sister chromatids (78). The following two mouse experiments suggest the critical role played by HJ resolvases in tumor suppression. SLX4 serves as docking sites for the MSH2, MUS81-EME1, SLX1-SLX4, and XPF-ERCC1 endonucleases (78). SLX4 plays a dominant role in preventing carcinogenesis, as evidenced by the data that the loss of SLX4 decreases a median survival time of mice to ~90 days due to enhanced tumorigenesis (79). The *MUS81* null mutation reduces the life expectancy of p53 null deficient mice by about 30% due to an increase in carcinogenesis (80). The critical role of MLH3 and PMS2 in the resolution of HJs emphasizes their strong tumor suppressor activities in addition to their function in MMR (21, 22, 81).

In this study, we characterized a major role of MLH3 and PMS2 in the DSB repair that is independent of MSH2 and MLH1. These results highlight an additional layer of the multifunctional role played by the MMR proteins (66). Studies on the molecular mechanisms of the process identified here will allow deciphering if this process is mediated by the homodimeric form of PMS2 and MLH3, complex with not yet characterized partners or a new pathway of DSB repair.

Experimental procedures

Cell clones

All the clones used in this study are summarized in Table 1.

Cell culture

Cell culture conditions for human TK6 cells was as described previously (82). Briefly, TK6 cells were grown in RPMI 1640 medium (Nacalai Tesque Inc., Kyoto, Japan) supplemented with 10% heat-inactivated horse serum (Gibco, Life technologies, New Zealand), 200 μg/ml sodium pyruvate and 100 U/ml penicillin -100 μg/ml streptomycin at 37^{O} C in 5% CO_2 atmosphere.

Generation of human PMS2$^{-/-}$ TK6 B cells

To generate a pair of TALEN expression plasmids against the *PMS2* gene, we used a Golden Gate TALEN kit and a TAL effector kit (Addgene, US) (83, 84). The TALEN target sites are shown in Figure S1A. The gene-targeting constructs were generated from the genomic DNA of TK6 cells by amplifying with primers *Hind*III-flanked F1 and *Hind*III -flanked R1 for the 5'-arm and *Xba*I-flanked F2 and *Xba*I-flanked R2 for the 3'-arm. The 5'-arm and 3'-arm PCR products were cloned into the corresponding sites of the DT-ApA/puro or DT-ApA/hygro vectors. 10 μg TALEN-expression plasmids and 10 μg linearized gene-targeting vectors were transfected into 10×10^6 TK6 cells using the Bio-Rad Gene Pulser II Transfection System at 250 V and 950 μF. After electroporation, cells were released into 20 ml drug-free medium containing 10% horse serum. 48 hours later, cells were seeded into 96-well plates with both hygromycin and puromycin antibiotics for two weeks. The gene disruption was confirmed by genomic PCR using primers P1, P2, P3, P4 (Figure S1B) and RT-qPCR using primers P5 and P6 (Figure S1C). All primers used in this study are shown in Table S1.

Generation of nuclease dead human PMS2$^{E705K/E705K}$ TK6 B cells

To generate nuclease dead human *PMS2*$^{E705K/E705K}$ TK6 B cells, we designed a guide RNA targeting intron sequence upstream of 12th exon using the Zhang CRISPR tool (85) and gene-targeting constructs. The CRISPR-target site is depicted in Figure S1C. The gene-targeting constructs were generated using SLiCE (Seamless Ligation Cloning Extract). The genomic DNA was amplified with primers F3 and R3 from the *PMS2*-gene locus and the PCR product was used as template DNA for amplifying the 5' arm. The 5'-arm was amplified using primers F4 and R4, where each primer shared 20-base pair-end homology with the insertion site of the vector. The sequence intended as the 3' arm of the *PMS2* targeting construct was amplified by PCR as two fragments using overlapping primers (F5 and R5) and that included a point mutation to change codon 705 from glutamic acid to lysine. The two fragments were then combined by chimeric PCR to yield the 3' targeting arm including the codon 705 mutation. The 3'-arm was amplified using primers F6 and R6, where each primer shared 20-base pair-end homology with the insertion site of the vector. Both vectors, DT-ApA/neo and DT-ApA/hygro, were linearized with *Not*I and *Xba*I. All the fragments of the vectors and inserts were purified using a QIAquick gel extraction kit (QIAGEN, Netherlands). The gene-targeting constructs were generated in a single reaction mixture containing DT-ApA/neo or DT-ApA/hygro vectors, 5'- and 3'-arms, and 2×SLiCE buffer (Invitrogen, US) and incubated for 30 min at room temperature. 6 μg of CRISPR and 2 μg of each gene-targeting vector were transfected into 4×10^6 TK6 cells using the Neon Transfection System (Life Technologies, US). After electroporation, cells were released into 20 ml drug-free medium containing 10% horse serum. Forty-eight hours later, cells were seeded into 96-well plates for selection with both neomycin and hygromycin antibiotics for two weeks. The gene disruption was confirmed by RT-PCR using primers F7 and R7 followed by direct sequencing (Figures S1D and S1E). The drug resistance markers are flanked by *lox*P sites, and were thus excised from *PMS2*$^{E705K/E705K}$ cells by transient expression of cre-recombinase, leading to the generation of *PMS2*$^{E705K/E705K}$ cells.

Generation of human MLH3$^{-/-}$ TK6 B cells

To disrupt the *MLH3* gene, we designed a guide RNA targeting the sixth exon using the Zhang CRISPR tool (85) and gene-targeting constructs. The CRISPR-target site is depicted in Figure S2A. The gene-targeting constructs were generated using SLiCE (Seamless Ligation Cloning Extract). The genomic DNA was amplified with primers F8 and R8 from the *MLH3*-gene locus and the PCR product was used as template DNA for amplifying the 5'- and 3'-arms. The 5'-arm was amplified using primers F9 and R9 and the 3'-arm was amplified using primers F10 and R10, where each primer shared 20-base pair-end homology with the insertion site of the vector. Both vectors, DT-

ApA/neo and DT-ApA/hygro, were linearized with *Afl*II and *Apa*I. All the fragments of the vectors and inserts were purified using a QIAquick gel extraction kit (QIAGEN, Netherlands). The gene-targeting constructs were generated in a single reaction mixture containing DT-ApA/neo or DT-ApA/hygro vectors, 5'- and 3'-arms, and 2×SLiCE buffer (Invitrogen, US) and incubated for 30 min at room temperature. 6 μg of CRISPR and 2 μg of each gene-targeting vector were transfected into 4×10^6 TK6 cells using the Neon Transfection System (Life Technologies, US). After electroporation, cells were released into 20 ml drug-free medium containing 10% horse serum. Forty-eight hours later, cells were seeded into 96-well plates for selection with both neomycin and hygromycin antibiotics for two weeks. The gene disruption was confirmed by RT-PCR using primers F11 and R11 (Figure S2B), and by Southern blot analysis with a 0.6 kb probe amplified by PCR from genomic DNA using F12 and R12 (Figure S2C). The genomic DNA of the candidate clones was digested with *Eco*RI for Southern blot analysis.

Generation of human MSH2$^{-/-}$ TK6 B cells

To disrupt the *MSH2* gene, we designed a guide RNA targeting the 4th exon using the Zhang CRISPR tool (85) and gene-targeting constructs. The CRISPR-target site is depicted in Figure S3A. The gene-targeting constructs were generated using SLiCE (Seamless Ligation Cloning Extract). The genomic DNA was amplified with primers F22 and R22 from the *MSH2*-gene locus and the PCR product was used as template DNA for amplifying the 5'- and 3'-arms. The 5'-arm was amplified using primers F23 and R23 and the 3'-arm was amplified using primers F24 and R24, where each primer shared 20-base pair-end homology with the insertion site of the vector. Both vectors, DT-ApA/neo and DT-ApA/puro, were linearized with *Afl*II and *Apa*I. All the fragments of the vectors and inserts were purified using a QIAquick gel extraction kit (QIAGEN, Netherlands). The gene-targeting constructs were generated in a single reaction mixture containing DT-ApA/neo or DT-ApA/puro vectors, 5'- and 3'-arms, and 2×SLiCE buffer (Invitrogen, US) and incubated for 30 min at room temperature. 6 μg of CRISPR and 2 μg of each gene-targeting vector were transfected into 4×10^6 TK6 cells using the Neon Transfection System (Life Technologies, US). After electroporation, cells were released into 20 ml drug-free medium containing 10% horse serum. Forty-eight hours later, cells were seeded into 96-well plates for selection with both neomycin and puromycin antibiotics for two weeks. The gene disruption was confirmed by genomic PCR using primers F25, F26 and R25 (Figure S3).

Generation of human MLH1$^{-/-}$ TK6 B cells

To disrupt the *MLH1* gene, we designed a guide RNA targeting the 8th exon using the Zhang CRISPR tool (85) and gene-targeting constructs. The CRISPR-target site is depicted in Figure S4A. The gene-targeting constructs were generated using SLiCE (Seamless Ligation Cloning Extract). The genomic DNA was amplified with primers F27 and R27 from the *MLH1*-gene locus and the PCR product was used as template DNA for amplifying the 5'- and 3'-arms. The 5'-arm was amplified using primers F28 and R28 and the 3'-arm was amplified using primers F29 and R29, where each primer shared 20-base pair-end homology with the insertion site of the vector. Both vectors, DT-ApA/neo and DT-ApA/puro, were linearized with *Afl*II and *Apa*I. All the fragments of the vectors and inserts were purified using a QIAquick gel extraction kit (QIAGEN, Netherlands). The gene-targeting constructs were generated in a single reaction mixture containing DT-ApA/neo or DT-ApA/puroro vectors, 5'- and 3'-arms, and 2×SLiCE buffer (Invitrogen, US) and incubated for 30 min at room temperature. 6 μg of CRISPR and 2 μg of each gene-targeting vector were transfected into 4×10^6 TK6 cells using the Neon Transfection System (Life Technologies, US). After electroporation, cells were released into 20 ml drug-free medium containing 10% horse serum. Forty-eight hours later, cells were seeded into 96-well plates for selection with both neomycin and puromycin antibiotics for two weeks. The gene disruption was confirmed by Southern blot analysis (genomic DNA was digested with *Sph*I) with a 0.52 kb probe amplified by PCR from genomic DNA using F30 and R30 (Figure S4B and S4C). The candidate clones were further confirmed by RT-PCR using primers F31 and R31 (Figure S4D) and Western blot analysis (Figure S4E).

Generation of human MUS81$^{-/-}$ TK6 B cells

To generate a pair of TALEN expression plasmids against the *MUS81* gene, we used a Golden Gate TALEN kit and a TAL effector kit (Addgene, US) (83, 84). The TALEN target sites are shown in Figure S5A. The gene-targeting constructs were generated from the genomic DNA of TK6 cells by amplifying with primers *Sac*I-flanked F19 and *Bam*HI-flanked R19 for the 5'-arm and *Bam*HI-flanked F20 and R20 for the 3'-arm. The 3'-arm PCR products were cloned into pCR-Blunt II-TOPO vector. The 5'-arm PCR products were cloned into the *Sac*I site of the pCR-Blunt II-TOPO vector containing 3'-arm. The *Bam*HI fragment containing either the *bsr^R* or *puro^R* gene was cloned into the *Bam*HI site between the 3'-arm and the 5'-arm in the pCR-Blunt II-TOPO vector. 10 μg TALEN-expression plasmids and 10 μg linearized gene-targeting vectors were transfected into 10×10^6 TK6 cells using the Bio-Rad Gene Pulser II Transfection System at 250 V and 950 μF. After electroporation, cells were released into 20 ml drug-free medium containing 10% horse

serum. 48 hours later, cells were seeded into 96-well plates with both blasticidin and puromycin antibiotics for two weeks. The genomic DNAs of the isolated clones resistant to both hygromycin and puromycin were digested with *Dra*I for Southern blot analysis. A 0.6 kb probe was generated by PCR of genomic DNA using primers F21 and R21 (Figure S5B).

Generation of nuclease dead human MLH3$^{D1223N/D1223N}$ and MLH3$^{E1229K/E1229K}$ TK6 B cells

To generate nuclease dead human *MLH3$^{EK/EK}$* and *MLH3$^{DN/DN}$* TK6 B cells, we designed a guide RNA targeting intron sequence upstream of seventh exon using the Zhang CRISPR tool (85) and gene-targeting constructs. The CRISPR-target site is depicted in Figure S6. The gene-targeting constructs were generated using SLiCE (Seamless Ligation Cloning Extract). The genomic DNA was amplified with primers F13 and R13 from the *MLH3*-gene locus and the PCR product was used as template DNA for amplifying the 5' arm. The 5'-arm was amplified using primers F14 and R14, where each primer shared 20-base pair-end homology with the insertion site of the vector. The sequence intended as the 3' arm of the *MLH3* targeting construct was amplified by PCR as two fragments using overlapping primers (F15 & R15 for *MLH3$^{DN/DN}$* and F16 & R16 for *MLH3$^{EK/EK}$* cells) and that included a point mutation to change codon from aspartic acid to asparagine (*MLH3$^{DN/DN}$*) and glutamic acid to lysine (*MLH3$^{EK/EK}$*) subsequently. The two fragments were then combined by chimeric PCR to yield the 3' targeting arm including the mutation. The 3'-arm was amplified using primers F17 and R17, where each primer shared 20-base pair-end homology with the insertion site of the vector. Both vectors, DT-ApA/neo and DT-ApA/hygro, were linearized with *Not*I and *Xba*I. All the fragments of the vectors and inserts were purified using a qiaquick gel extraction kit (QIAGEN, Netherlands). The gene-targeting constructs were generated in a single reaction mixture containing DT-ApA/neo or DT-ApA/hygro vectors, 5'- and 3'-arms, and 2×SLiCE buffer (Invitrogen, US) and incubated for 30 min at room temperature. 6 μg of CRISPR and 2 μg of each gene-targeting vector were transfected into 4×10^6 TK6 cells using the Neon Transfection System (Life Technologies, US). After electroporation, cells were released into 20 ml drug-free medium containing 10% horse serum. Forty-eight hours later, cells were seeded into 96-well plates for selection with both neomycin and hygromycin antibiotics for two weeks. The site directed mutagenesis was confirmed by genomic PCR using primers F18 and R18 followed by direct sequencing (Figures S6C and D). The drug resistance markers are flanked by *lox*P sites, and were thus excised from *MLH3$^{DN/DN}$* and *MLH3$^{EK/EK}$* cells by transient expression of cre-recombinase, leading to the generation of *MLH3$^{DN/DN}$* and *MLH3$^{EK/EK}$* cells.

Colony-survival assay

To measure sensitivity, cells were treated with camptothecin (Topogen, Inc, US), olaparib (Funakoshi, Japan) and irradiated with ionizing radiation (^{137}Cs). Cell sensitivity to these DNA-damaging agents was evaluated by counting colony formation in methylcellulose plates as described previously (86).

Heteroallelic crossover analysis

The human lymphoblastoid cell line TSCER2 is a TK6 derivative with an I-*Sce*1 site inserted into the TK locus (50, 51). TSCER2 cells are compound heterozygous ($TK^{-/-}$) for a point mutation in exons 4 and 5. DSB occurring at the I-*Sce*1 site results in homologous recombination between the alleles and produces TK-proficient revertants ($TK^{+/-}$). 4×10^6 TK6 cells were transfected with 6 μg I-*Sce*1 expression vector using the Neon Transfection System (Life Technologies, US) with 3X pulse at 1350 V and with 10 msec pulse width and released into 20 ml drug-free medium containing 10% horse serum. After 48 hours, cells were seeded as $1x10^6$ cells per 96-well plates, with 2'-deoxycytidine (Sigma D0776), hypoxanthine (Sigma H9377), aminopterin (Sigma A3411) and thymidine (Sigma T9250) (CHAT for TK-revertants) medium. Drug resistant colonies were counted 2 weeks later.

Chromosomal aberrations analysis

TK6 cells were irradiated with 1 Gy of IR. The cells were then treated with 0.1 μg/ml colcemid (GIBCO-BRL, Grand Island, NY) and incubated at 37^{O} C for 3 hours. Experimental conditions for chromosomal aberration analysis were as described previously (72). Briefly, harvested cells were treated with 1 ml of 75 mM KCl for 15 min at room temperature and fixed in 5 ml of a freshly prepared 3:1 mixture of methanol/acetic acid. The cell suspension was dropped onto a glass slide and air-dried. The slides were stained with 5% Giemsa solution (NacalaiTesque) for 10 min and air-dried after being rinsed carefully with water. All chromosomes in each mitotic cell were scored at 1,000× magnifications. A total of 50 mitotic cells were scored for each group using a microscope.

Sister chromatid exchange (SCE) analysis

TK6 cells were incubated with or without cisplatin (2 μM). After one hour, cells were washed and released into BrdU (100 mM) containing media. Cells were incubated for 2 more cell cycle and

treated with Colcemid (0.1 mg/ml) for 3 hours before being harvested. Metaphase chromosomes were prepared and assayed for SCEs as previously described (64).

Immunostaining and microscopic analysis

Cells were fixed with 4% paraformaldehyde (Nacalai Tesque, Japan) for 10 min at room temperature and permeabilized with 0.5% TritonX-100 (Sigma, St. Louis, US) for 30 min. Images were taken with a confocal microscope (TCS SP8, Leica Microsystems, Germany).

Antibodies

Anti-γH2AX mouse monoclonal (1:1000, Millipore, US); anti-Rad51 rabbit polyclonal (1:500, Sigma, US); anti-MLH1: (1:1000, ab92312, abcam); anti-FLAG: (1:500, F1804, Sigma); Mouse monoclonal α–β–Tubulin (Sigma,US); alexa fluor 488-conjugated anti-mouse IgG (1:1000, Molecular Probes); alexa fluor 488–conjugated anti-rabbit IgG (1:1000, Molecular Probes); Goat monoclonal a-mouse HRP(Invitrogen, US)

Construction of Flag-tagged hGen1 with nuclear localization signal expressing TK6 cell lines

Flag-tagged hGen1-NES (4A)-NLS^{+} expressing TK6 cells were generated using a genetically modified retroviral vector as described (Figure S7) (72). Briefly, the coding sequence for hGen1-NES (4A)-3xNLS^{+}-3xFlag was cloned into the pMSCV retroviral expression vector (Clontech) (Figure S7A). The newly engineered retroviral expression vector was co-transfected into human 293T cells with a helper plasmid (pClampho) expressing the viral gag, pol and env proteins to produce viral supernatant. The viral supernatant was collected after 48h and used to transduce into *wild-type*, $PMS2^{EK/EK}$, $MLH3^{DN/DN}$, $PMS2^{EK/EK}/MLH3^{DN/DN}$, $MUS81^{-/-}$, and $RAD54^{-/-}$ TK6 mutant strains (Figure S7B). The efficiency of each step was assessed by quantifying the number of cells expressing GFP (Figure S7C). The expression of hGen1-NES (4A)-3xNLS^{+}-3xFlag was further confirmed by western blot (WB). Experimental conditions for WB analysis were as described previously (87). The following antibodies were used: anti-Flag antibody for overnight at 4°C and anti-mouse IgG HRP-linked antibody for 1h at room temperature was used as the primary and secondary antibodies respectively (Figure S7D).

Quantification and Statistical Analysis

For all statistical analyses with a p-value, unpaired Student's t-test was used. Error bars represent standard deviation (SD), as indicated in the legends. We calculated the propagation of errors using the following formula: $\sqrt{((\text{SD with IR treatment})^2 + (\text{SD without IR treatment}))^2}$

Acknowledgments

We wish to thank A. Noguchi, A. Kobayashi, and M. Kato for their technical assistance and the lab members for their stimulating discussions.

Conflict of interest

None declared.

References

1. Lyer, R. R., Pluciennik, A., Burdett, V., and Modrich, P. L. (2006) DNA mismatch repair: Functions and mechanisms. *Chemical Reviews*. **106**, 302–323
2. Jiricny, J. (2006) The multifaceted mismatch-repair system. *Nature reviews. Molecular cell biology*. **7**, 335–46
3. Hoffmann, E. R., and Borts, R. H. (2004) Meiotic recombination intermediates and mismatch repair proteins. *Cytogenetic and Genome Research*. **107**, 232–248
4. Modrich, P., and Lahue, R. (1996) Mismatch repair in replication fidelity, genetic recombination, and cancer biology. *Annual review of biochemistry*. **65**, 101–33
5. Kunkel, T. A., and Erie, D. A. (2015) Eukaryotic Mismatch Repair in Relation to DNA Replication. *Annual Review of Genetics*. **49**, 291–313
6. Harfe, B. D., and Jinks-Robertson, S. (2000) DNA mismatch repair and genetic instability. *Annual review of genetics*. **34**, 359–399
7. Kolodner, R. D., and Marsischky, G. T. (1999) Eukaryotic DNA mismatch repair. *Current opinion in genetics & development*. **9**, 89–96
8. Marsischky, G. T., Filosi, N., Kane, M. F., and Kolodner, R. (1996) Redundancy of Saccharomyces cerevisiae MSH3 and MSH6 in MSH2-dependent mismatch repair. *Genes and Development*. **10**, 407–420

9. Sia, E. A., Kokoska, R. J., Dominska, M., Greenwell, P., and Petes, T. D. (1997) Microsatellite instability in yeast: dependence on repeat unit size and DNA mismatch repair genes. *Molecular and cellular biology*. **17**, 2851–8

10. Srivatsan, A., Bowen, N., and Kolodner, R. D. (2014) Mispair-specific recruitment of the Mlh1-Pms1 complex identifies repair substrates of the Saccharomyces cerevisiae Msh2-Msh3 complex. *Journal of Biological Chemistry*. **289**, 9352–9364

11. Goellner, E. M., Putnam, C. D., and Kolodner, R. D. (2015) Exonuclease 1-dependent and independent mismatch repair. *DNA repair*. **32**, 24–32

12. Flores-Rozas, H., and Kolodner, R. D. (1998) The Saccharomyces cerevisiae MLH3 gene functions in MSH3-dependent suppression of frameshift mutations. *Proceedings of the National Academy of Sciences of the United States of America*. **95**, 12404–9

13. N Matton 1, J Simonetti, K. W. (2000) Identification of mismatch repair protein complexes in HeLa nuclear extracts and their interaction with heteroduplex DNA. *Journal of Biological Chemistry*, **275**, 17808-17813.

14. Gueneau, E., Dherin, C., Legrand, P., Tellier-Lebegue, C., Gilquin, B., Bonnesoeur, P., Londino, F., Quemener, C., Le Du, M.-H., Márquez, J. a, Moutiez, M., Gondry, M., Boiteux, S., and Charbonnier, J.-B. (2013) Structure of the MutLα C-terminal domain reveals how Mlh1 contributes to Pms1 endonuclease site. *Nature structural & molecular biology*. 10.1038/nsmb.2511

15. Kadyrov, F. A., Dzantiev, L., Constantin, N., and Modrich, P. (2006) Endonucleolytic function of MutLalpha in human mismatch repair. *Cell*. **126**, 297–308

16. de Wind, N., Dekker, M., Berns, A., Radman, M., and te Riele, H. (1995) Inactivation of the mouse Msh2 gene results in mismatch repair deficiency, methylation tolerance, hyperrecombination, and predisposition to cancer. *Cell*. **82**, 321–330

17. Elliott, B., and Jasin, M. (2001) Repair of Double-Strand Breaks by Homologous Recombination in Mismatch Repair-Defective Mammalian Cells. **21**, 2671–2682

18. Sharma, S., Doherty, K. M., and Brosh, R. M. (2006) Mechanisms of RecQ helicases in pathways of DNA metabolism and maintenance of genomic stability. *Biochemical Journal*. **398**, 319–337

19. Bannister, L. A., Waldman, B. C., and Waldman, A. S. (2004) Modulation of error-prone double-strand break repair in mammalian chromosomes by DNA mismatch repair protein Mlh1. *DNA Repair*. 10.1016/j.dnarep.2004.01.001

20. Shibata, A., Conrad, S., Birraux, J., Geuting, V., Barton, O., Ismail, A., Kakarougkas, A., Meek, K., Taucher-Scholz, G., Löbrich, M., and Jeggo, P. a (2011) Factors determining DNA double-strand break repair pathway choice in G2 phase. *The EMBO journal*. **30**, 1079–92

21. Zakharyevich, K., Tang, S., Ma, Y., and Hunter, N. (2012) Delineation of joint molecule resolution pathways in meiosis identifies a crossover-specific resolvase. *Cell*. **149**, 334–347

22. Toledo, M., Sun, X., Brieño-Enríquez, M. A., Raghavan, V., Gray, S., Pea, J., Milano, C. R., Venkatesh, A., Patel, L., Borst, P. L., Alani, E., and Cohen, P. E. (2019) A mutation in the endonuclease domain of mouse MLH3 reveals novel roles for mutlγ during crossover formation in meiotic prophase I. *PLoS Genetics*. 10.1371/journal.pgen.1008177

23. Baker, S. M., Bronner, C. E., Zhang, L., Plug, A. W., Robatzek, M., Warren, G., Elliott, E. A., Yu, J., Ashley, T., Arnheim, N., Flavell, R. A., and Liskay, R. M. (1995) Male mice defective in the DNA mismatch repair gene PMS2 exhibit abnormal chromosome synapsis in meiosis. *Cell*. **82**, 309–319

24. Baker, S. M., Plug, a W., Prolla, T. a, Bronner, C. E., Harris, a C., Yao, X., Christie, D. M., Monell, C., Arnheim, N., Bradley, a, Ashley, T., and Liskay, R. M. (1996) Involvement of mouse Mlh1 in DNA mismatch repair and meiotic crossing over. *Nature genetics*. **13**, 336–342

25. Edelmann, W., Cohen, P. E., Kane, M., Lau, K., Morrow, B., Bennett, S., Umar, A., Kunkel, T., Cattoretti, G., Chaganti, R., Pollard, J. W., Kolodner, R. D., and Kucherlapati, R. (1996) Meiotic pachytene arrest in MLH1-deficient mice. *Cell*. **85**, 1125–1134

26. Lipkin, S. M., Moens, P. B., Wang, V., Lenzi, M., Shanmugarajah, D., Gilgeous, A., Thomas, J., Cheng, J., Touchman, J. W., Green, E. D., Schwartzberg, P., Collins, F. S., and Cohen, P. E. (2002) Meiotic arrest and aneuploidy in MLH3-deficient mice. *Nature genetics*. **31**, 385–390

27. Svetlanov, A., Baudat, F., Cohen, P. E., and De Massy, B. (2008) Distinct functions of MLH3 at recombination hot spots in the mouse. *Genetics*. **178**, 1937–1945

28. Fischer, J. M., Dudley, S., Miller, A. J., and Liskay, R. M. (2016) An intact Pms2 ATPase domain is not essential for male fertility. *DNA Repair*. **39**, 46–51

29. Elda Cannavo, Aurore Sanchez, Roopesh Anand, Lepakshi Ranjha, Jannik Hugener, Céline Adam, Ananya Acharya, Nicolas Weyland, Xavier Aran-Guiu, Jean-Baptiste Charbonnier,

Eva R. Hoffmann, Valérie Borde, J. M. & P. C. (2020) Regulation of the MLH1–MLH3 endonuclease in meiosis. *Nature*. https://doi.org/10.1038/s41586-020-2592-2

30. Hunter, N., Kulkarni, D., Owens, S., Honda, M., Ito, M., Yang, Y., Corrigan, M., Chen, L., and Quan, A. (2020) PCNA activates the MutLγ endonuclease to promote meiotic crossing over. *Nature*. https://doi.org/10.1038/s41586-020-2645-6

31. Takeda, S., Nakamura, K., Taniguchi, Y., and Paull, T. T. (2007) Ctp1/CtIP and the MRN Complex Collaborate in the Initial Steps of Homologous Recombination. *Molecular Cell*. **28**, 351–352

32. Bernstein, K. A., and Rothstein, R. (2009) At Loose Ends: Resecting a Double-Strand Break. *Cell*. **137**, 807–810

33. Mehta, A., and Haber, J. E. (2014) Sources of DNA double-strand breaks and models of recombinational DNA repair. *Cold Spring Harbor Perspectives in Biology*

34. Sugawara, N., Wang, X., and Haber, J. E. (2003) In vivo roles of Rad52, Rad54, and Rad55 proteins in Rad51-mediated recombination. *Molecular Cell*. **12**, 209–219

35. Dion, V., Kalck, V., Horigome, C., Towbin, B. D., and Gasser, S. M. (2012) Increased mobility of double-strand breaks requires Mec1, Rad9 and the homologous recombination machinery. *Nature Cell Biology*. **14**, 502–509

36. Schwartz, E. K., and Heyer, W. D. (2011) Processing of joint molecule intermediates by structure-selective endonucleases during homologous recombination in eukaryotes. *Chromosoma*. **120**, 109–127

37. West, S. C., Blanco, M. G., Chan, Y. W., Matos, J., Sarbajna, S., and Wyatt, H. D. M. (2015) Resolution of Recombination Intermediates: Mechanisms and Regulation. *Cold Spring Harbor Symposia on Quantitative Biology*. **LXXX**, 027649

38. Wyatt, H. D. M., Laister, R. C., Martin, S. R., Arrowsmith, C. H., and West, S. C. (2017) The SMX DNA Repair Tri-nuclease. *Molecular Cell*. **65**, 848-860.e11

39. Kikuchi, K., Narita, T., Pham, V. T., Iijima, J., Hirota, K., Keka, I. S., Mohiuddin, Okawa, K., Hori, T., Fukagawa, T., Essers, J., Kanaar, R., Whitby, M. C., Sugasawa, K., Taniguchi, Y., Kitagawa, K., and Takeda, S. (2013) Structure-specific endonucleases Xpf and Mus81 play overlapping but essential roles in DNA repair by homologous recombination. *Cancer Research*. **73**, 4362–4371

40. Abraham, J., Lemmers, B., Hande, M. P., Moynahan, M. E., Chahwan, C., Ciccia, A.,

Essers, J., Hanada, K., Chahwan, R., Khaw, A. K., McPherson, P., Shehabeldin, A., Laister, R., Arrowsmith, C., Kanaar, R., West, S. C., Jasin, M., and Hakem, R. (2003) Eme1 is involved in DNA damage processing and maintenance of genomic stability in mammalian cells. *EMBO Journal*. **22**, 6137–6147

41. McPherson, J. P., Lemmers, B., Chahwan, R., Pamidi, A., Migon, E., Matysiak-Zablocki, E., Moynahan, M. E., Essers, J., Hanada, K., Poonepalli, A., Sanchez-Sweatman, O., Khokha, R., Kanaar, R., Jasin, M., Hande, M. P., and Hakem, R. (2004) Involvement of mammalian Mus81 in genome integrity and tumor suppression. *Science*. **304**, 1822–1826

42. Castor, D., Nair, N., Déclais, A. C., Lachaud, C., Toth, R., Macartney, T. J., Lilley, D. M. J., Arthur, J. S. C., and Rouse, J. (2013) Cooperative control of holliday junction resolution and DNA Repair by the SLX1 and MUS81-EME1 nucleases. *Molecular Cell*. **52**, 221–233

43. Wang Xiaowen, Wang Herui, Guo Bin, Zhang Ya, Gong Yinv, Zhang Chi, Xu Hong, and W. X. (2016) Gen1 and Eme1 Play Redundant Roles in DNA Repair and Meiotic Recombination in Mice. *DNA and Cell Biology*

44. Kaur, H., DeMuyt, A., and Lichten, M. (2015) Top3-Rmi1 DNA single-strand decatenase is integral to the formation and resolution of meiotic recombination intermediates. *Molecular Cell*. **57**, 583–594

45. Tang, S., Wu, M. K. Y., Zhang, R., and Hunter, N. (2015) Pervasive and essential roles of the top3-rmi1 decatenase orchestrate recombination and facilitate chromosome segregation in meiosis. *Molecular Cell*. **57**, 607–621

46. Takata, M., Sasaki, M. S., Sonoda, E., Morrison, C., Hashimoto, M., Utsumi, H., Yamaguchi-Iwai, Y., Shinohara, A., and Takeda, S. (1998) Homologous recombination and non-homologous end-joining pathways of DNA double-strand break repair have overlapping roles in the maintenance of chromosomal integrity in vertebrate cells. *EMBO Journal*. **17**, 5497–5508

47. Keka, I. S., Mohiuddin, Maede, Y., Rahman, M. M., Sakuma, T., Honma, M., Yamamoto, T., Takeda, S., and Sasanuma, H. (2015) Smarcal1 promotes double-strand-break repair by nonhomologous end-joining. *Nucleic Acids Research*. 10.1093/nar/gkv621

48. Murai, J., Huang, S. Y. N., Das, B. B., Renaud, A., Zhang, Y., Doroshow, J. H., Ji, J., Takeda, S., and Pommier, Y. (2012) Trapping of PARP1 and PARP2 by clinical PARP inhibitors. *Cancer Research*. **72**, 5588–5599

49. Fowler, P., Whitwell, J., Jeffrey, L., Young, J., Smith, K., and Kirkland, D. (2010) Cadmium

chloride, benzo[a]pyrene and cyclophosphamide tested in the in vitro mammalian cell micronucleus test (MNvit) in the human lymphoblastoid cell line TK6 at Covance laboratories, Harrogate UK in support of OECD draft Test Guideline 487. *Mutation Research*. **702**, 171–174

50. Honma, M., Izumi, M., Sakuraba, M., Tadokoro, S., Sakamoto, H., Wang, W., Yatagai, F., and Hayashi, M. (2003) Deletion, Rearrangement, and Gene Conversion; Genetic Consequences of Chromosomal Double-Strand Breaks in Human Cells. *Environmental and Molecular Mutagenesis*. **42**, 288–298

51. Neuwirth, E. a H., Honma, M., and Grosovsky, A. J. (2007) Interchromosomal crossover in human cells is associated with long gene conversion tracts. *Molecular and cellular biology*. **27**, 5261–5274

52. Yoshimoto, K., Mizoguchi, M., Hata, N., Murata, H., Hatae, R., Amano, T., Nakamizo, A., and Sasaki, T. (2012) Complex DNA repair pathways as possible therapeutic targets to overcome temozolomide resistance in glioblastoma. *Frontiers in oncology*. **2**, 186

53. Cejka, P., Stojic, L., Mojas, N., Russell, A. M., Heinimann, K., Cannavó, E., Di Pietro, M., Marra, G., and Jiricny, J. (2003) Methylation-induced G2/M arrest requires a full complement of the mismatch repair protein hMLH1. *EMBO Journal*. **22**, 2245–2254

54. Kadyrov, F. A., Holmes, S. F., Arana, M. E., Lukianova, O. A., O'Donnell, M., Kunkel, T. A., and Modrich, P. (2007) Saccharomyces cerevisiae MutLalpha is a mismatch repair endonuclease. *The Journal of biological chemistry*. **282**, 37181–90

55. Desch??nes, S. M., Tomer, G., Nguyen, M., Erdeniz, N., Juba, N. C., Sep??lveda, N., Pisani, J. E., and Michael Liskay, R. (2007) The E705K mutation in hPMS2 exerts recessive, not dominant, effects on mismatch repair. *Cancer Letters*. **249**, 148–156

56. Nishant, K. T., Plys, A. J., and Alani, E. (2008) A mutation in the putative MLH3 endonuclease domain confers a defect in both mismatch repair and meiosis in Saccharomyces cerevisiae. *Genetics*. **179**, 747–755

57. Kadyrova, L. Y., Gujar, V., Burdett, V., Modrich, P. L., and Kadyrov, F. A. (2020) Human MutLγ, the MLH1–MLH3 heterodimer, is an endonuclease that promotes DNA expansion. *Proceedings of the National Academy of Sciences of the United States of America*. **117**, 3535–3542

58. Al-Sweel, N., Raghavan, V., Dutta, A., Ajith, V. P., Di Vietro, L., Khondakar, N., Manhart, C. M., Surtees, J. A., Nishant, K. T., and Alani, E. (2017) *Mlh3 Mutations in Baker'S Yeast*

Alter Meiotic Recombination Outcomes By Increasing Noncrossover Events Genome-Wide. PLoS genetics, **13**, e1007067

59. Sanchez, A., Adam, C., Rauh, F., Duroc, Y., Ranjha, L., Lombard, B., Mu, X., Loew, D., Keeney, S., Cejka, P., Guérois, R., Klein, F., Charbonnier, J.-B., and Borde, V. (2020) Mechanism of in vivo activation of the MutLγ-Exo1 complex for meiotic crossover formation. *bioRxiv*. 10.1101/2019.12.16.876623

60. Hoa, N. N., Akagawa, R., Yamasaki, T., Hirota, K., Sasa, K., Natsume, T., Kobayashi, J., Sakuma, T., Yamamoto, T., Komatsu, K., Kanemaki, M. T., Pommier, Y., Takeda, S., and Sasanuma, H. (2015) Relative contribution of four nucleases, CtIP, Dna2, Exo1 and Mre11, to the initial step of DNA double-strand break repair by homologous recombination in both the chicken DT40 and human TK6 cell lines. *Genes to Cells*. 10.1111/gtc.12310

61. Fujita, M., Sasanuma, H., Yamamoto, K. N., Harada, H., Kurosawa, A., Adachi, N., Omura, M., Hiraoka, M., Takeda, S., and Hirota, K. (2013) Interference in DNA Replication Can Cause Mitotic Chromosomal Breakage Unassociated with Double-Strand Breaks. *PLoS ONE*

62. Wechsler, T., Newman, S., and West, S. C. (2011) Aberrant chromosome morphology in human cells defective for Holliday junction resolution. *Nature*. **471**, 642–646

63. Suzuki, T., Yasui, M., and Honma, M. (2016) Mutator Phenotype and DNA Double-Strand Break Repair in BLM Helicase-Deficient Human Cells. *Molecular and Cellular Biology*. **36**, 2877–2889

64. Sonoda, E., Sasaki, M. S., Morrison, C., Yamaguchi-Iwai, Y., Takata, M., and Takeda, S. (1999) Sister chromatid exchanges are mediated by homologous recombination in vertebrate cells. *Molecular and cellular biology*. **19**, 5166–9

65. Wyatt, H. D. M., Sarbajna, S., Matos, J., and West, S. C. (2013) Coordinated actions of SLX1-SLX4 and MUS81-EME1 for holliday junction resolution in human cells. *Molecular Cell*. **52**, 234–247

66. Jiricny, J. (2013) Postreplicative mismatch repair. *Cold Spring Harbor Perspectives in Biology*. **5**, 1–23

67. Söding, J., Biegert, A., and Lupas, A. N. (2005) The HHpred interactive server for protein homology detection and structure prediction. *Nucleic Acids Research*. **33**, 244–248

68. Zimmermann, L., Stephens, A., Nam, S. Z., Rau, D., Kübler, J., Lozajic, M., Gabler, F.,

Söding, J., Lupas, A. N., and Alva, V. (2018) A Completely Reimplemented MPI Bioinformatics Toolkit with a New HHpred Server at its Core. *Journal of Molecular Biology*. **430**, 2237–2243

69. Song, Y., Dimaio, F., Wang, R. Y. R., Kim, D., Miles, C., Brunette, T., Thompson, J., and Baker, D. (2013) High-resolution comparative modeling with RosettaCM. *Structure*. **21**, 1735–1742

70. Lorenz, A., West, S. C., and Whitby, M. C. (2010) The human Holliday junction resolvase GEN1 rescues the meiotic phenotype of a Schizosaccharomyces pombe mus81 mutant. *Nucleic acids research*. **38**, 1866–73

71. Chan, Y. W., and West, S. C. (2014) Spatial control of the GEN1 Holliday junction resolvase ensures genome stability. *Nature communications*. **5**, 4844

72. Mohiuddin, Keka, I. S., Evans, T. J., Hirota, K., Shimizu, H., Kono, K., Takeda, S., and Hirano, S. (2014) A novel genotoxicity assay of carbon nanotubes using functional macrophage receptor with collagenous structure (MARCO)-expressing chicken B lymphocytes. *Archives of Toxicology*. **88**, 145–160

73. Zeng, M., Narayanan, L., Xu, X. S., Prolla, T. A., Liskay, R. M., and Glazer, P. M. (2000) Ionizing radiation-induced apoptosis via separate Pms2- and p53-dependent pathways. *Cancer Research*. **60**, 4889–4893

74. Shcherbakova, P. V, Hall, M. C., Lewis, M. S., Bennett, S. E., Martin, K. J., Bushel, P. R., Afshari, C. A., and Kunkel, T. A. (2001) Inactivation of DNA mismatch repair by increased expression of yeast MLH1. *Molecular and cellular biology*. 10.1128/MCB.21.3.940-951.2001

75. Chen, P. C., Dudley, S., Hagen, W., Dizon, D., Paxton, L., Reichow, D., Yoon, S. R., Yang, K., Arnheim, N., Liskay, R. M., and Lipkin, S. M. (2005) Contributions by MutL homologues Mlh3 and Pms2 to DNA mismatch repair and tumor suppression in the mouse. *Cancer Research*. **65**, 8662–8670

76. Sarbajna, S., Davies, D., and West, S. C. (2014) Roles of SLX1-SLX4, MUS81-EME1, and GEN1 in avoiding genome instability and mitotic catastrophe. *Genes and Development*. **28**, 1124–1136

77. Garner, E., Kim, Y., Lach, F. P., Kottemann, M. C., and Smogorzewska, A. (2013) Human GEN1 and the SLX4-Associated Nucleases MUS81 and SLX1 Are Essential for the Resolution of Replication-Induced Holliday Junctions. *Cell Reports*. **5**, 207–215

78. West, S. C., and Chan, Y. W. (2017) Genome Instability as a Consequence of Defects in the Resolution of Recombination Intermediates. *Cold Spring Harbor symposia on quantitative biology*. **82**, 207–212

79. Hodskinson, M. R. G., Silhan, J., Crossan, G. P., Garaycoechea, J. I., Mukherjee, S., Johnson, C. M., Sch??rer, O. D., and Patel, K. J. (2014) Mouse SLX4 Is a Tumor Suppressor that Stimulates the Activity of the Nuclease XPF-ERCC1 in DNA Crosslink Repair. *Molecular Cell*. **54**, 472–484

80. Pamidi, A., Cardoso, R., Hakem, A., Matysiak-Zablocki, E., Poonepalli, A., Tamblyn, L., Perez-Ordonez, B., Hande, M. P., Sanchez, O., and Hakem, R. (2007) Functional interplay of p53 and Mus81 in DNA damage responses and cancer. *Cancer Research*. **67**, 8527–8535

81. Wang, T. F., Kleckner, N., and Hunter, N. (1999) Functional specificity of MutL homologs in yeast: Evidence for three Mlh1-based heterocomplexes with distinct roles during meiosis in recombination and mismatch correction. *Proceedings of the National Academy of Sciences of the United States of America*. **96**, 13914–13919

82. Mohiuddin, M., Evans, T. J., Rahman, M. M., Keka, I. S., Tsuda, M., Sasanuma, H., and Takeda, S. (2018) SUMOylation of PCNA by PIAS1 and PIAS4 promotes template switch in the chicken and human B cell lines. *Proceedings of the National Academy of Sciences of the United States of America*. 10.1073/pnas.1716349115

83. Cermak, T., Doyle, E., and Christian, M. (2011) Efficient design and assembly of custom TALEN and other TAL effector-based constructs for DNA targeting. *Nucleic acids …*. **39**, e82

84. Sakuma, T., Ochiai, H., Kaneko, T., Mashimo, T., Tokumasu, D., Sakane, Y., Suzuki, K., Miyamoto, T., Sakamoto, N., Matsuura, S., and Yamamoto, T. (2013) Repeating pattern of non-RVD variations in DNA-binding modules enhances TALEN activity. *Scientific reports*. **3**, 3379

85. Ran, F. A., Hsu, P. D., Lin, C. Y., Gootenberg, J. S., Konermann, S., Trevino, A. E., Scott, D. A., Inoue, A., Matoba, S., Zhang, Y., and Zhang, F. (2013) Double nicking by RNA-guided CRISPR cas9 for enhanced genome editing specificity. *Cell*. **154**, 1380–1389

86. Mohiuddin, M., Rahman, M. M., Sale, J. E., and Pearson, C. E. (2019) CtIP-BRCA1 complex and MRE11 maintain replication forks in the presence of chain terminating nucleoside analogs. *Nucleic acids research*. 10.1093/nar/gkz009

87. Mohiuddin, Kobayashi S, Keka IS, Guilbaud G, Sale J, Narita T, Abdel-Aziz HI, Wang X,

Ogawa S, Sasanuma H, Chiu R,Oestergaard VH, Lisby M, T. S. (2016) The role of HERC2 and RNF8 ubiquitin E3 ligases in the promotion of translesion DNA synthesis in the chicken DT40 cell line. *DNA Repair (Amst).* . **40**, 67-76.

Table 1. Panel of cell line used in this study

Genotype	Parental Cell line	Marker genes	References
PMS2$^{-/-}$	TK6	hygro^{R}, puro^{R}	♯ T
PMS2$^{EK/EK}$	TK6	-	♯ C
MLH3$^{-/-}$	TK6	hygro^{R}, neo^{R}	♯ C
MLH3$^{DN/DN}$	TK6	-	♯ C
MLH3$^{EK/EK}$	TK6	-	♯ C
PMS2$^{EK/EK}$ *MLH3*$^{DN/DN}$	TK6	-	♯ C
PMS2$^{EK/EK}$ *MLH3*$^{EK/EK}$	TK6	-	♯ C
MUS81$^{-/-}$	TK6	bsr^{R}, puro^{R}	♯ T
RAD54$^{-/-}$	TK6	neo^{R}, puro^{R}	T (47)
MLH1$^{-/-}$	TK6	hygro^{R}, puro^{R}	♯ C
MSH2$^{-/-}$	TK6	neo^{R}, puro^{R}	♯ C

♯ = This study; T = TALEN; C = CRISPR

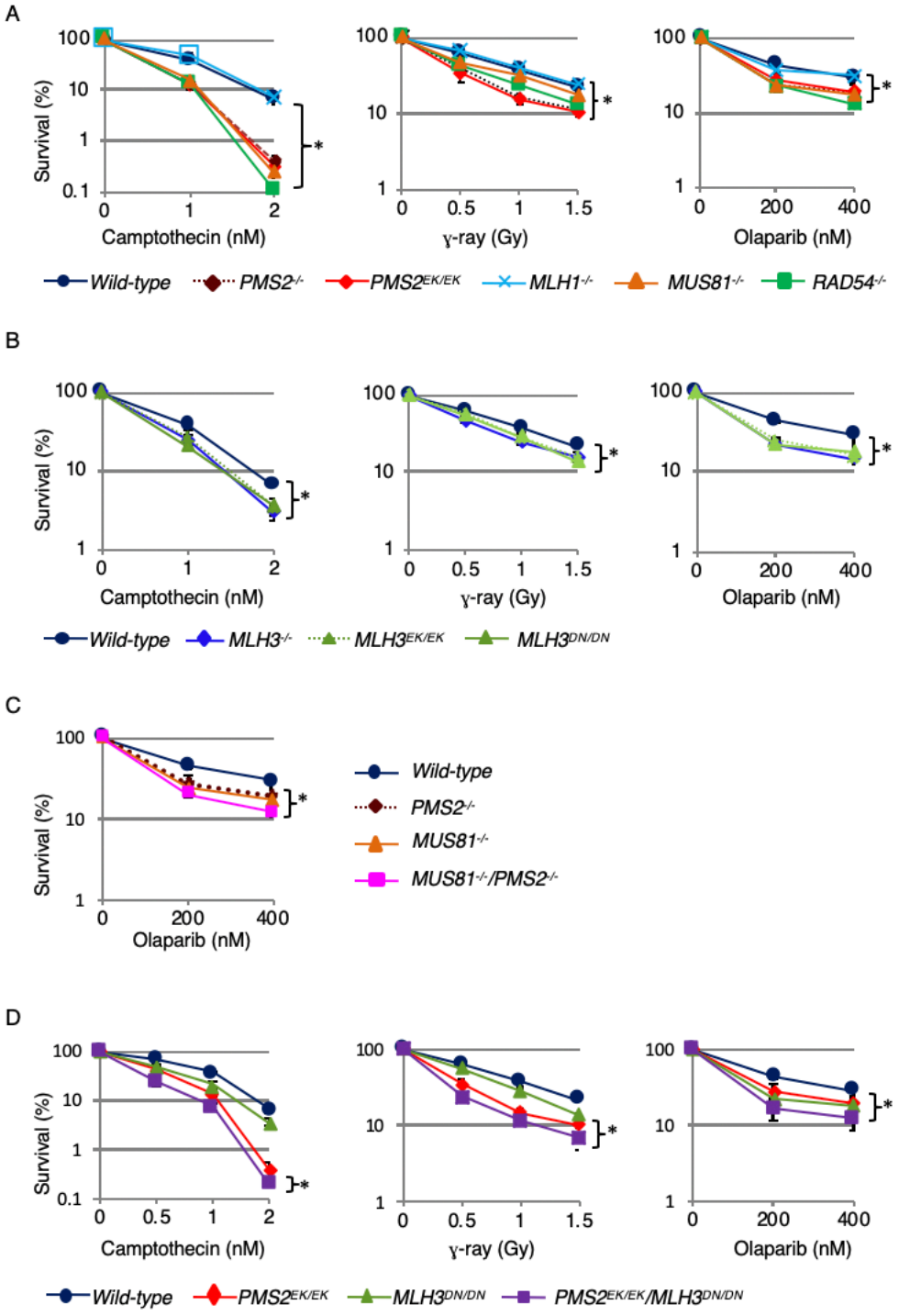
A
Survival (%)
Camptothecin (nM)
γ-ray (Gy)
Olaparib (nM)
Wild-type
PMS2-/-
PMS2EK/EK
MLH1-/-
MUS81-/-
RAD54-/-
B
MLH3-/-
MLH3EK/EK
MLH3DN/DN
C
MUS81-/-/PMS2-/-
D
PMS2EK/EK/MLH3DN/DN

Figure 1. *MLH3* and *PMS2* mutants are sensitive to camptothecin, γ-rays and olaparib. (**A**) Clonogenic cell survival assay following exposure of *PMS2* mutants to Camptothecin, γ-rays and olaparib (PARP inhibitor). The *x*-axis represents the dose of the indicated DNA-damaging agent on a linear scale; the *y*-axis represents the survival fraction on a logarithmic scale. Error bars show the SD of the mean for three independent assays. Statistical analyses were performed by student's t-test (**P*<0.01). (**B**) Clonogenic cell survival assay following exposure of *MLH3* mutants to Camptothecin, γ-rays and olaparib (PARP inhibitor). Cellular sensitivity is shown as in figure A. Statistical analyses were performed by student's t-test (**P*<0.01). (**C**) Clonogenic cell survival assay following exposure of $MUS81^{-/-}PMS2^{-/-}$ mutants to olaparib (PARP inhibitor). Cellular sensitivity is shown as in figure A. (**D**) $PMS2^{EK/EK}/MLH3^{DN/DN}$ double mutant cells show stronger HR defects than $PMS2^{EK/EK}$ and $MLH3^{DN/DN}$ cells. Clonogenic cell survival assay following exposure of $PMS2^{EK/EK}$, $MLH3^{DN/DN}$, $PMS2^{EK/EK}MLH3^{DN/DN}$ mutants to Camptothecin, γ-rays and olaparib (PARP inhibitor). Cellular sensitivity is shown as in figure 1A. Statistical analyses were performed by student's t-test (**P*<0.05).

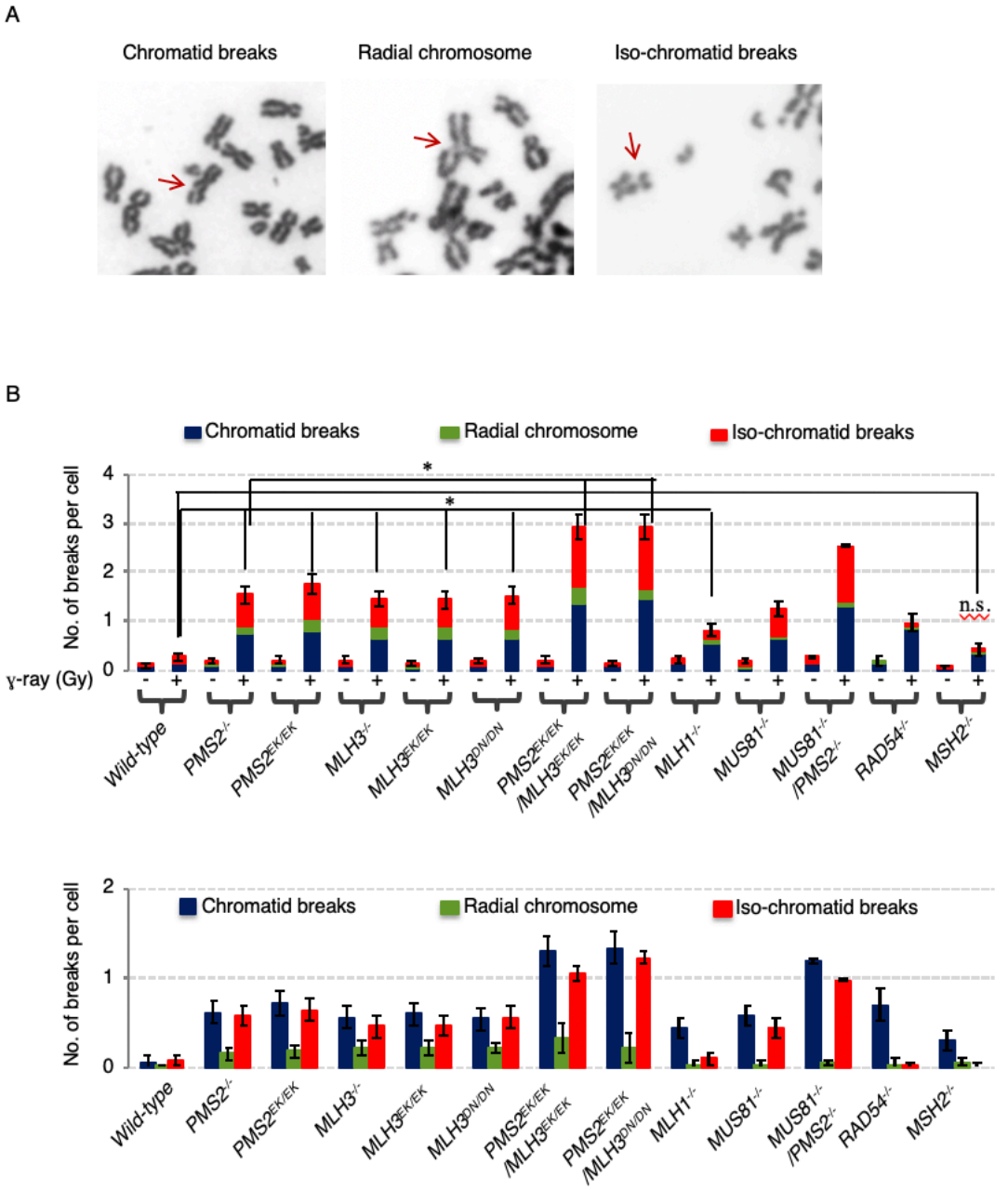

Figure 2. HR-mediated repair of □-ray-induced DSBs is severely compromised in the PMS2 and MLH3 mutant cells. (**A**) Representative images of chromatid breaks, isochromatid breaks and radial chromosome after irradiation of 1 Gy IR. **(B)** Number of breaks per mitotic cells in the indicated genotypes (Upper panel). Error bars represent standard deviation. The asterisks indicate $P < 0.001$, calculated by Student's t test. At least 50 mitotic cells were counted for each cell line.

The subtracted numbers of breaks before the exposure from breaks after the exposure (Lower panel). Error bars represent propagation of error.

Maminur, et al., Figure 3

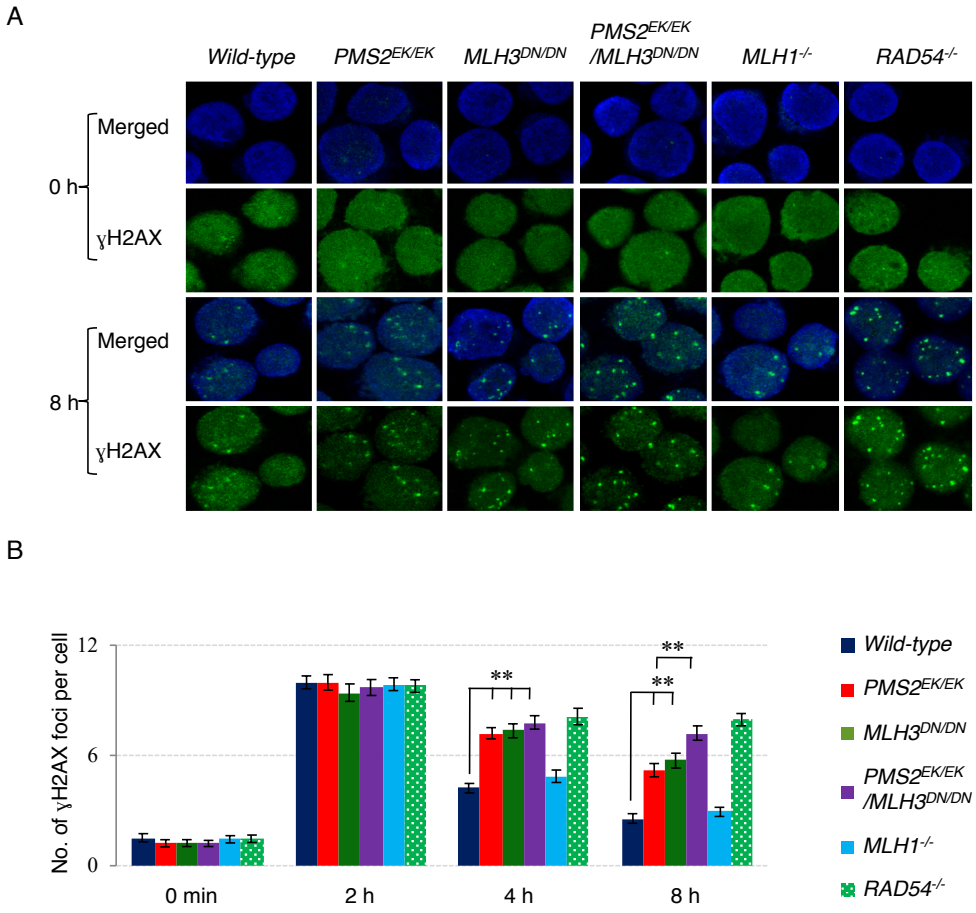

Figure. 3 Following ionizing radiation, γH2AX foci appear with normal kinetics but persist for longer time in the *PMS2* and *MLH3* mutants in comparison with wild-type cells. (**A**) Representative fluorescence microscopic images of γH2AX foci in the indicated cell lines before and 8 h after irradiation of 1 Gy IR. (**B**) Quantification of γH2AX foci number per cell at indicated time points. At least 100 cells were counted per condition in each experiment. Statistical analyses were performed by student's t-test (**P<0.001).

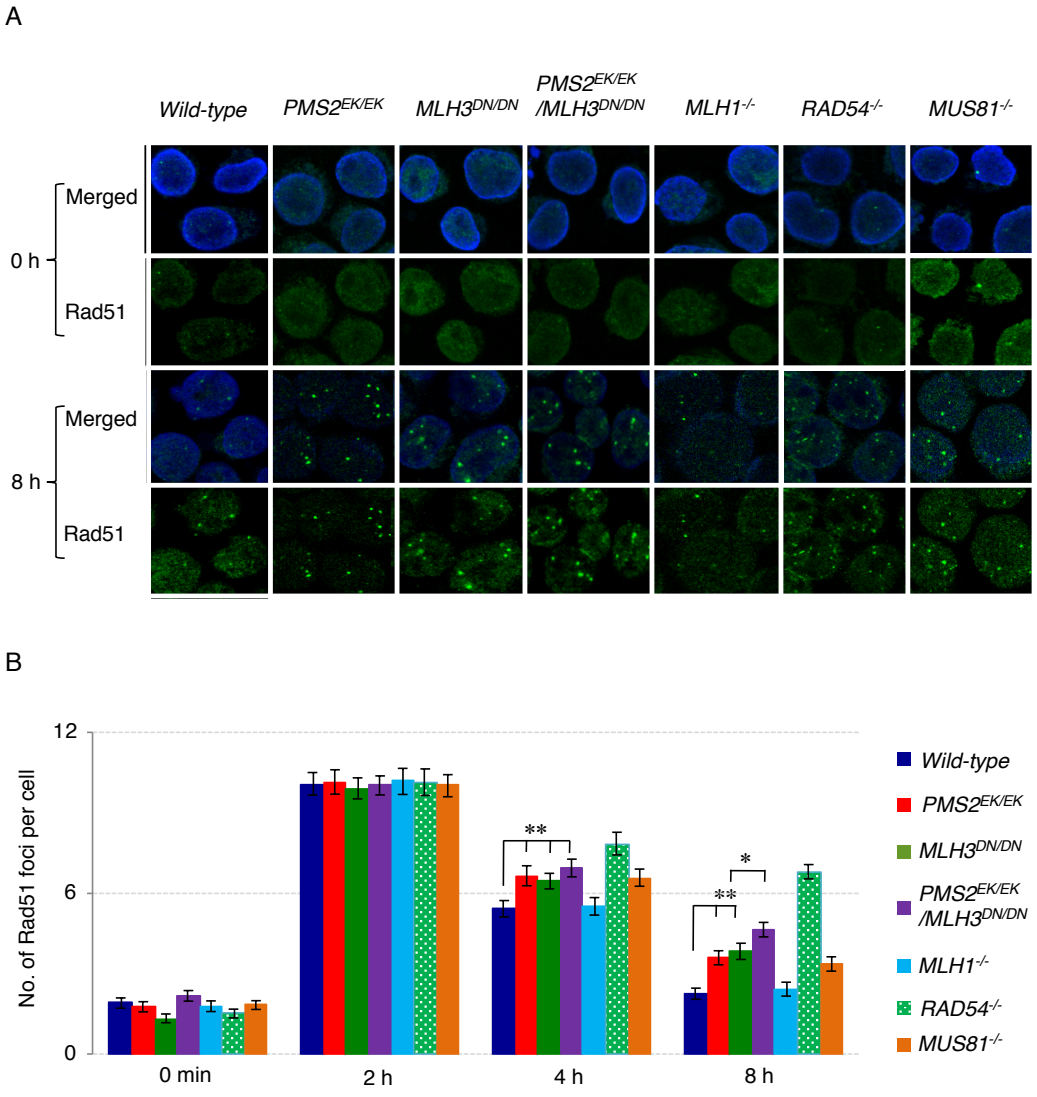

Figure. 4 Following ionizing radiation, Rad51 foci appear with normal kinetics but persist for longer time in the *PMS2* and *MLH3* mutants in comparison with wild-type cells. (**A**) Representative fluorescence microscopic images of Rad51 foci in the indicated cell lines before and 8 h after irradiation of 1 Gy IR. (**B**) Quantification of Rad51 foci number per cell at indicated time points. At least 100 cells were counted per condition in each experiment. Statistical analyses were performed by student's t-test (**P*<0.01 and (***P*<0.001).

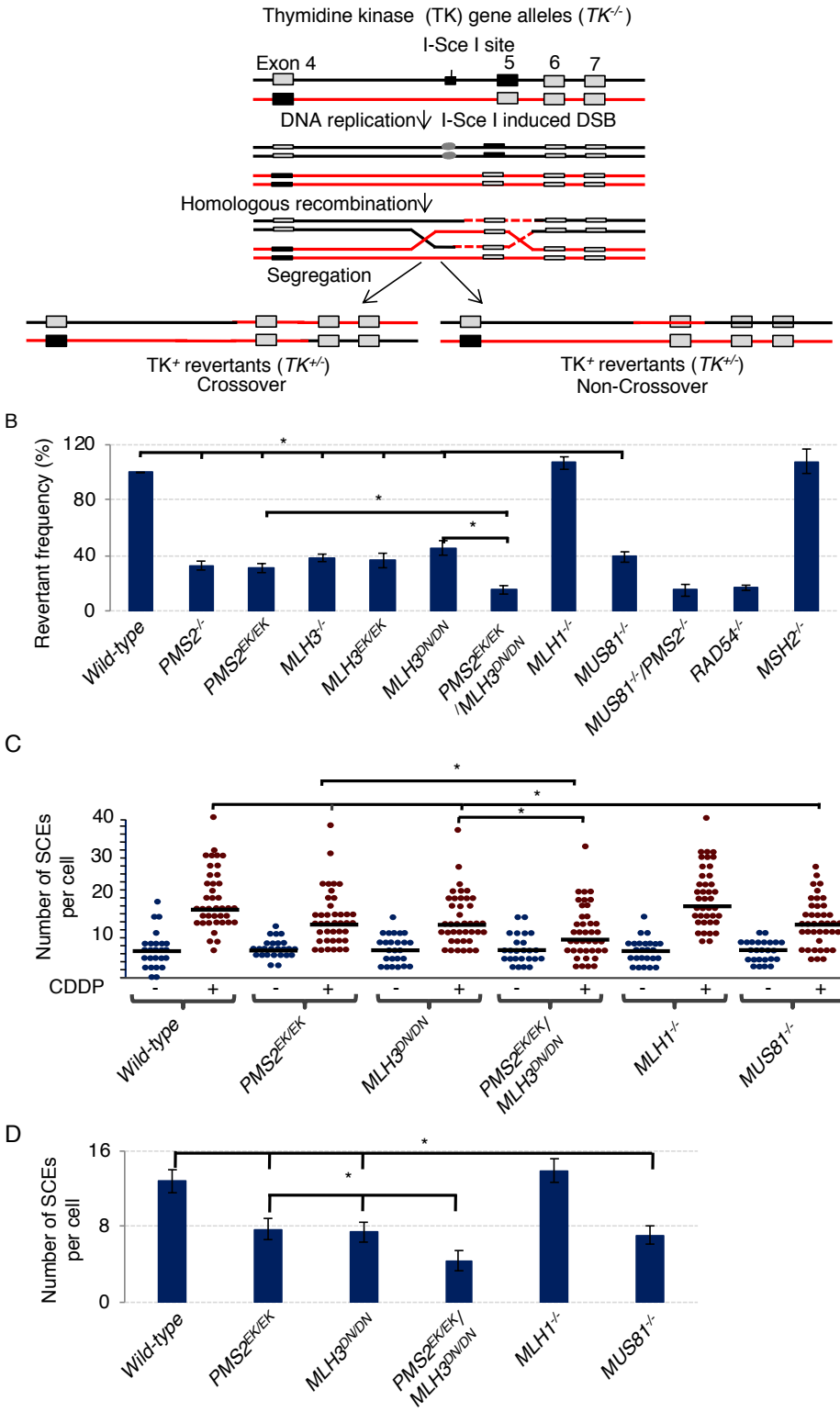
A
Thymidine kinase (TK) gene alleles (TK-/-)
I-Sce I site
Exon 4
5
6
7
DNA replication
I-Sce I induced DSB
Homologous recombination
Segregation
TK+ revertants (TK+/-)
Crossover
TK+ revertants (TK+/-)
Non-Crossover
B
Revertant frequency (%)
120
80
40
0
Wild-type
PMS2-/-
PMS2EK/EK
MLH3-/-
MLH3EK/EK
MLH3DN/DN
PMS2EK/EK /MLH3DN/DN
MLH1-/-
MUS81-/-
MUS81-/-/PMS2-/-
RAD54-/-
MSH2-/-
C
Number of SCEs per cell
40
30
20
10
CDDP
-
+
Wild-type
PMS2EK/EK
MLH3DN/DN
PMS2EK/EK/ MLH3DN/DN
MLH1-/-
MUS81-/-
D
Number of SCEs per cell
16
8
0
Wild-type
PMS2EK/EK
MLH3DN/DN
PMS2EK/EK/ MLH3DN/DN
MLH1-/-
MUS81-/-

Figure 5. *MLH3*$^{DN/DN}$ and *PMS2*$^{EK/EK}$ cells are deficient in HR associated with crossover. (**A**) Schematic diagram showing DSB-repair events that repair I-*Sce*1-induced DSBs in the endogenous thymidine kinase (*TK*) locus. *TK*$^{-/-}$ cells carry an I-*Sce*1 site in intronic sequences of the *TK* allelic gene. The site of mutations in the *TK* allelic genes are marked as closed rectangles at exon 4 and exon 5. When a DSB at the I-*Sce*I site is repaired by HR, TK-proficient revertants (TK$^{+/-}$) are generated by crossover resolution from TSCER2 cells under CHAT selection. (**B**) Histogram representing the frequency of DSB-repair events (*y*-axis) in the indicated genotypes (*x*-axis). Error bars indicate SD of more than three independent experiments. Statistical analyses were performed by student's t-test (P<0.01). (**C**) Nuclease dead *PMS2* and *MLH3* mutants displayed reduced number of sister chromatid exchange (SCE) events induced by cisplatin (CDDP). The distribution of SCE events per 100 chromosomes is shown for the indicated cell types. Mean values for SCE before and after exposure to the DNA damaging agents are indicated. Statistical analyses were performed by student's t-test (P<0.01). (**D**) The subtracted numbers of SCEs before the exposure from SCEs after the exposure. Error bars indicate SEM. Statistical analyses were performed by student's t-test (P<0.01).

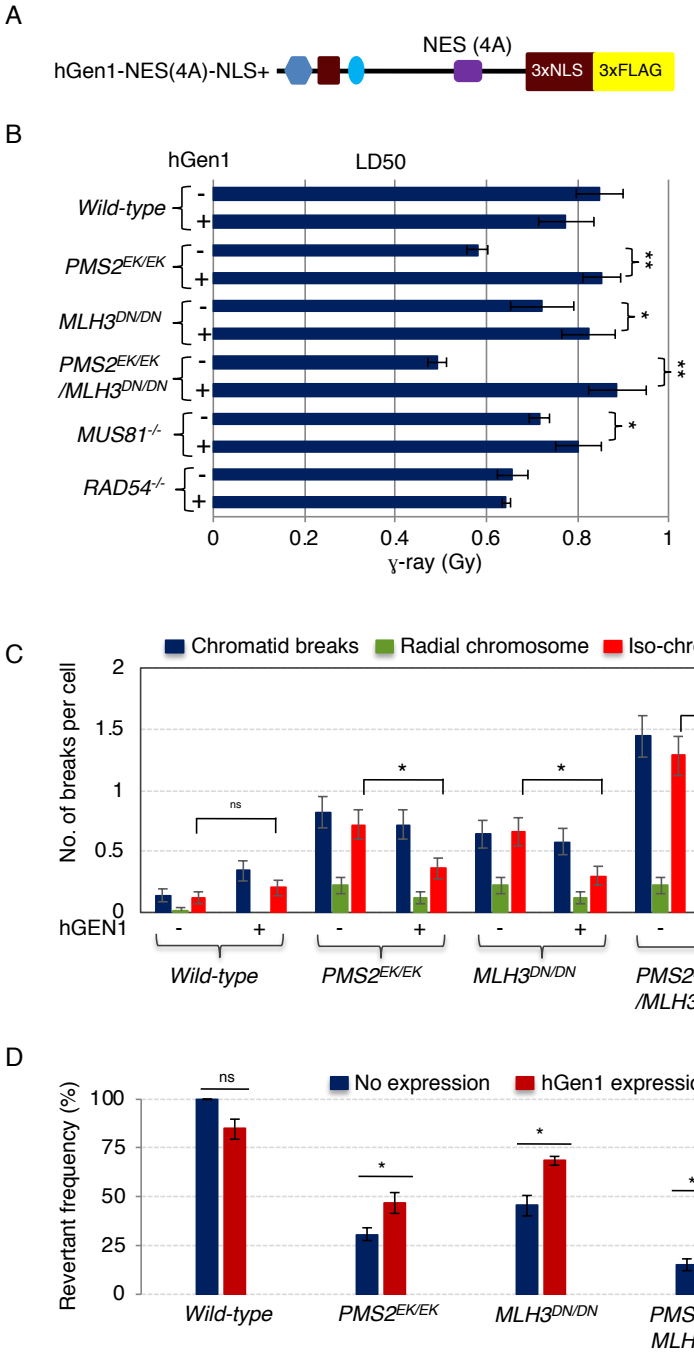
A
hGen1-NES(4A)-NLS+
NES (4A)
3xNLS
3xFLAG
B
hGen1
LD50
Wild-type
PMS2EK/EK
MLH3DN/DN
PMS2EK/EK /MLH3DN/DN
MUS81-/-
RAD54-/-
0
0.2
0.4
0.6
0.8
1
γ-ray (Gy)
C
Chromatid breaks
Radial chromosome
Iso-chromatid breaks
No. of breaks per cell
hGEN1
ns
Wild-type
PMS2EK/EK
MLH3DN/DN
PMS2EK/EK /MLH3DN/DN
MUS81-/-
D
No expression
hGen1 expression
Revertant frequency (%)
Wild-type
PMS2EK/EK
MLH3DN/DN
PMS2EK/EK/ MLH3DN/DN
MUS81-/-

Figure 6. Significant rescue of the defective HR of the *MLH3* and *PMS2* mutants by ectopic expression of GEN1. (**A**) Schematic representation of hGEN1 with a mutated NES and 3xNLS sequences. (**B**) Clonogenic cell survival to the indicated DNA-damaging agents was analyzed as described in Figure 1A. Lethal dose 50% (LD50) is the concentration of DNA damaging agents that reduces cellular survival to 50% relative to cells non-treated with DNA damaging agents. Error bars show the standard deviation of the mean of at least three independent experiments. Statistical analyses were performed by student's t-test (**P*<0.05 and (***P*<0.01). (**C**) Number of IR-induced chromosomal aberrations per mitotic cells in the indicated genotypes. Error bars represent standard deviation. At least 50 mitotic cells were counted for each cell line. Statistical analyses were performed by student's t-test (**P*<0.05 and (***P*<0.01). (**D**) Frequency of heteroallelic HR, associated with crossover was measured and calculated as described in Figure 5B. Statistical analyses were performed by student's t-test (**P*<0.05 and (***P*<0.01).